Device

Article

# Discrimination of extracellular miRNA sources for the identification of tumor-related functions based on nanowire thermofluidics

## Graphical abstract

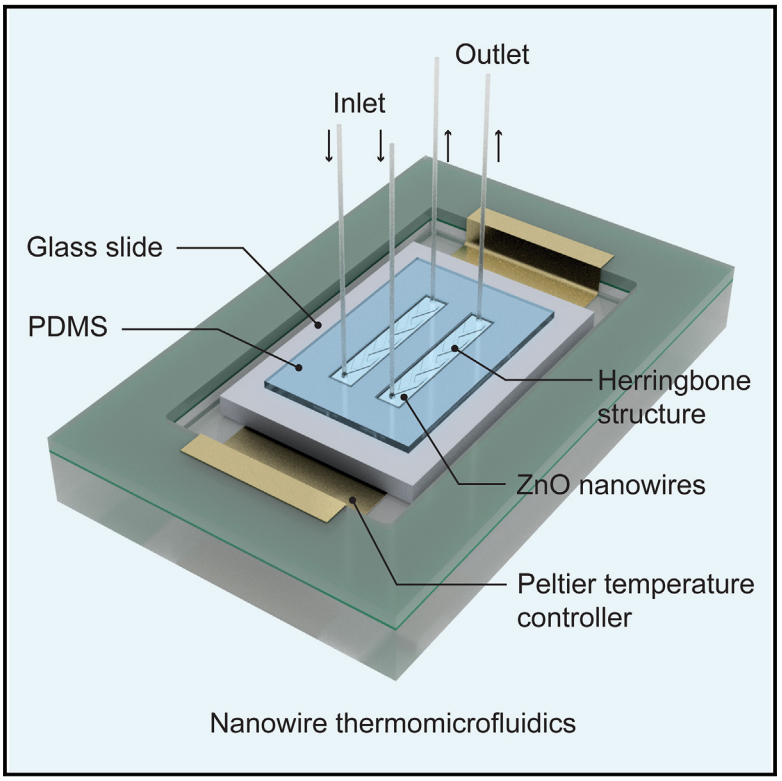


## Highlights

- EV miRNAs and EV-free miRNAs are discriminated using NW thermomicrofluidics
- miRNA sources and tumor-related functions are identified and matched
- A small volume (50 μL) and a short time (35 min) for miRNA extraction are required

## Authors

Kunanon Chattrairat, Akira Yokoi, Min Zhang, ..., Hiroaki Kajiyama, Yoshinobu Baba, Takao Yasui

## Correspondence

chattrairat.k.aa@m.titech.ac.jp (K.C.), ayokoi@med.nagoya-u.ac.jp (A.Y.), babaymtt@chembio.nagoya-u.ac.jp (Y.B.), yasuit@bio.titech.ac.jp (T.Y.)

## In brief

MicroRNAs (miRNAs) are potential diagnostic and prognostic tools for cancer. Our nanowire (NW) thermomicrofluidic device integrated with a Peltier temperature controller captures and extracts miRNAs from ovarian cancer serum and discriminates sources of the miRNAs, either inside or outside extracellular vesicles (EVs). We also discovered during the test that oncogenesis miRNAs are inside the EVs and tumor-suppressor miRNAs are on the outside. Our NW thermomicrofluidics offers an opportunity to develop miRNA analytical systems with high precision and accuracy.

4 Validate
Functional device with real-world testing, ready to scale

Chattrairat et al., 2024, Device 2, 100363
June 21, 2024 
https://doi.org/10.1016/j.device.2024.100363

CellPress

Please cite this article in press as: Chattrairat et al., Discrimination of extracellular miRNA sources for the identification of tumor-related functions based on nanowire thermofluidics, Device (2024), https://doi.org/10.1016/j.device.2024.100363

Device

CellPress
OPEN ACCESS

Article

# Discrimination of extracellular miRNA sources for the identification of tumor-related functions based on nanowire thermofluidics

Kunanon Chattrairat,[1,2,3,*] Akira Yokoi,[4,5,6,*] Min Zhang,[2] Mikiko Iida,[2] Kosuke Yoshida,[4,5] Masami Kitagawa,[4,7] Ayuka Niwa,[8] Masatoshi Maeki,[9,10] Takeshi Hasegawa,[11] Takeshi Yokoyama,[12,13] Yoshikazu Tanaka,[12,13] Yusuke Miyazaki,[14]

*(Author list continued on next page)*

[1]Department of Biomolecular Engineering, Graduate School of Engineering, Nagoya University, Furo-cho, Chikusa-ku, Nagoya 464-8603, Japan
[2]Institute of Nano-Life-Systems, Institutes of Innovation for Future Society, Nagoya University, Furo-cho, Chikusa-ku, Nagoya 464-8603, Japan
[3]Department of Life Science and Technology, Tokyo Institute of Technology, Nagatsuta 4259, Midori-ku, Yokohama 226-8501, Japan
[4]Department of Obstetrics and Gynecology, Nagoya University Graduate School of Medicine, Tsurumai-cho 65, Showa-ku, Nagoya 466-8550, Japan
[5]Nagoya University Institute for Advanced Research (IAR), Furo-cho, Chikusa-ku, Nagoya 464-8601, Japan
[6]Japan Science and Technology Agency (JST), FOREST, Saitama, Japan
[7]Bell Research Center, Department of Obstetrics and Gynecology Collaborative Research, Graduate School of Medicine, Nagoya University, Nagoya, Japan
[8]Graduate School of Chemical Sciences and Engineering, Hokkaido University, Kita 13 Nishi 8, Kita-ku, Sapporo 060-8628, Japan
[9]Division of Applied Chemistry, Faculty of Engineering, Hokkaido University, Kita 13 Nishi 8, Kita-ku, Sapporo 060-8628, Japan
[10]Japan Science and Technology Agency (JST), PRESTO, 4-1-8 Honcho, Kawaguchi, Saitama 332-0012, Japan
[11]Institute for Chemical Research, Kyoto University, Uji, Kyoto 611-0011, Japan

*(Affiliations continued on next page)*

**THE BIGGER PICTURE** MicroRNAs (miRNAs) have tumor regulation functions, such as oncogenesis; thus, they are prospective biomarkers for diagnosis and prognosis. Conventional methods cannot discriminate within a single sample between miRNAs contained in extracellular vesicles (EVs) (i.e., EV miRNAs) and those that are not (i.e., EV-free miRNAs). Here, we construct a nanowire (NW) thermomicrofluidic device integrated with a Peltier temperature controller for discriminating between the two main sources of miRNAs and showcase its diagnostic ability using ovarian cancer serum. Our statistical analysis identified a relationship between miRNA sources and tumor-related functions of the miRNAs: that oncogenesis miRNAs are inside the EVs and tumor-suppressor miRNAs are outside. The NW thermomicrofluidics provides a simple, rapid, and effective method for miRNA extraction and paves the way for future miRNA extraction methods as diagnostic and prognostic tools.

## SUMMARY

MicroRNAs (miRNAs) are prospective biomarkers for diagnosis and prognosis due to their specific functions. Conventional methods lack the ability to discriminate two main miRNA sources—extracellular vesicle (EV) miRNAs and EV-free miRNAs (i.e., miRNAs not contained in EVs)—in one sample. Here, we demonstrate that a nanowire (NW) thermomicrofluidic device integrated with a Peltier temperature controller can capture EVs and EV-free miRNAs and then preferentially release the EV-free miRNAs by thermal energy and extract the EV miRNAs via a lysis buffer. This leads to discrimination between EV miRNAs and EV-free miRNAs from ovarian cancer serum. Statistical analysis identified a relationship between miRNA source and tumor-related functions of the miRNAs: oncogenesis miRNAs were inside the EVs, and tumor-suppressor miRNAs were outside them. We demonstrate that the NW thermomicrofluidics provides the advantages of a simple, rapid, and effective method for miRNA extraction, accompanied by information from inside or outside the EVs.

CellPress
OPEN ACCESS

Device
Article

Wataru Shinoda,[14] Manabu Tokeshi,[2,9,15] Kazuki Nagashima,[10,16] Takeshi Yanagida,[17] Hiroaki Kajiyama,[4] Yoshinobu Baba,[1,2,15,*] and Takao Yasui[1,2,3,10,15,18,*]

[12]Graduate School of Life Sciences, Tohoku University, 2-1-1 Katahira, Aoba-ku, Sendai 980-8577, Japan
[13]The advanced center for innovations in next-generation medicine (INGEM), Tohoku University, 2-1 Seriryo-machi, Aoba-ku, Sendai, 980-8573, Japan
[14]Research Institute for Interdisciplinary Science, Okayama University, Okayama 700-8530, Japan
[15]Institute of Quantum Life Science, National Institutes for Quantum Science and Technology (QST), Anagawa 4-9-1, Inage-ku, Chiba 263-8555, Japan
[16]Research Institute for Electronic Science (RIES), Hokkaido University, N21W10 (or Kita 21 Nishi 10), Kita-ku, Sapporo 001-0020, Japan
[17]Department of Applied Chemistry, Graduate School of Engineering, The University of Tokyo, 7-3-1 Hongo, Bunkyo-ku, Tokyo 113-8656, Japan
[18]Lead contact
*Correspondence: chattrairat.k.aa@m.titech.ac.jp (K.C.), ayokoi@med.nagoya-u.ac.jp (A.Y.), babaymtt@chembio.nagoya-u.ac.jp (Y.B.), yasuit@bio.titech.ac.jp (T.Y.)
https://doi.org/10.1016/j.device.2024.100363

## INTRODUCTION

MicroRNAs (miRNAs) are small endogenous noncoding RNAs, ranging between 18 and 24 nucleotides in length, and have been reported as biomarkers for disease diagnosis due to their specific functions in biological systems.[1] miRNAs control cellular protein expression by binding to the 3′ untranslated region (UTR) of target messenger RNAs,[2] where the 3′ carbon of the sugar molecule is located in the nucleic acid backbone. In addition, they have been mentioned as having the potential to serve as noninvasive biomarkers for cancer diagnosis and prognosis.[3] Extracellular miRNAs in body fluids are considered mostly to be contained in extracellular vesicles (EVs), which are bilayers composed of phospholipids,[4,5] but EV-free miRNAs (i.e., miRNAs not contained in EVs) have also been found in body fluids.[6] Some of the EV-free miRNAs may bind to proteins of the Argonaute (AGO) family or to lipoproteins, e.g., high-density lipoproteins (HDLs) and low-density lipoproteins (LDLs).[7–9] A previous study using high-resolution iodixanol density gradient purification reported that AGO proteins were strongly associated with nonvesicular fractions that were independent components of small EVs.[10] Therefore, extracellular miRNA sources are divided into two main sources: miRNAs encapsulated in EVs (EV miRNAs)[6] and EV-free miRNAs.[8] Although extensive investigations have been conducted on the functions of miRNAs, the relationship between the sources of miRNAs and tumor-related functions remains to be determined. Conventional methods for miRNA extraction are unable to discriminate the miRNA sources in a single sample, and a method for miRNA extraction followed by miRNA source discrimination between the two miRNA sources is necessary to classify and reveal essential and specific extracellular miRNA information.

Information on whether the miRNA is inside or outside the EVs is important for better understanding of miRNA functions, biogenesis, and pathways, but there is no reported technique to extract EV miRNAs and EV-free miRNAs separately from a single sample. On the other hand, techniques for extracting EV miRNAs or EV-free miRNAs separately have been reported. A standard technique for isolating EVs from biological fluids is ultracentrifugation (UC), which is easy to use and does not require a long pre-treatment of samples. Recently, several commercial kits have become available to isolate EVs based on precipitation and/or application of columns. The EV-free miRNAs have been extracted from biological fluids by using immunoprecipitation and isopycnic density gradient UC.[7,11] However, none of the previous methods can separate and recover EV miRNAs and EV-free miRNAs from a single sample, because each method inevitably discards or contaminates one of the miRNA sources to isolate the other one. In cases where there is a considerable quantity of the sample, such as a cell culture medium, the sample can be divided into two parts, one to isolate EVs and the other to isolate EV-free miRNAs, which may not be possible for smaller sample volumes. Previously, we have demonstrated that nanowires (NWs) had the ability to collect both EVs and EV-free miRNAs, and large numbers of cancer-related miRNAs could be obtained from urine samples.[12,13] In the present work, we conceived the idea of adding a heating mechanism to the NW microfluidics to preferentially desorb EV-free miRNAs due to the difference in the capture strength of EVs and EV-free miRNAs on NWs caused by the difference in their molecular structures.

We achieved miRNA source discrimination by a technique to extract EV miRNAs and EV-free miRNAs separately using an NW thermomicrofluidic device. We used zinc oxide NWs in the NW thermomicrofluidics to demonstrate the ability to capture EVs and EV-free miRNAs onto NWs as previously reported.[12–17] Then, the NW thermomicrofluidics released the EV-free miRNAs preferentially by thermal energy, which was followed by extracting EV miRNAs *in situ* by introducing a lysis buffer. We applied the NW thermomicrofluidics to small-volume ovarian cancer serum samples to realize short-time miRNA extraction that contained information from inside or outside the EVs. From the information, we identified whether miRNAs with tumor-related miRNA functions were inside or outside the EVs.

## RESULTS

### Working principle for miRNA discrimination

The NW microfluidics with the herringbone structure[18] was integrated with the Peltier temperature controller to provide the external thermal energy, allowing separation and recovery of EV miRNAs and EV-free miRNAs. Upper and lower thermocouples measured the temperatures above and below the NW microfluidic substrate with high accuracy. The miRNA extraction was accompanied by information from inside or outside the EVs and it consisted of three steps (Figure 1). In the first step, NWs in the NW thermomicrofluidics captured both EVs and EV-free miRNAs, and

Please cite this article in press as: Chattrairat et al., Discrimination of extracellular miRNA sources for the identification of tumor-related functions based on nanowire thermofluidics, Device (2024), https://doi.org/10.1016/j.device.2024.100363





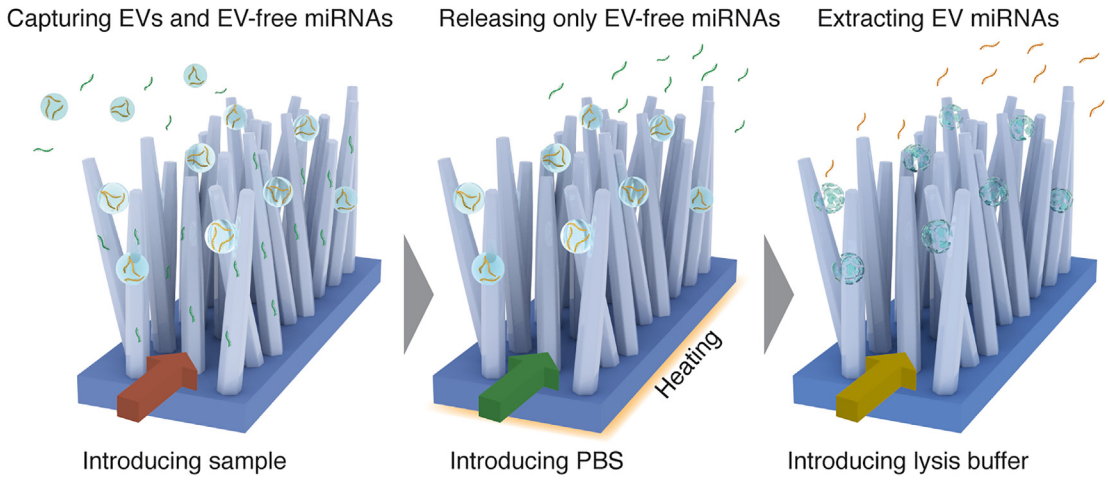


**Figure 1. Schematic images of the NW thermomicrofluidics and miRNA discrimination and extraction steps**

After a sample is introduced, the NW thermomicrofluidics capture both EVs and EV-free miRNAs. Next, during heating, PBS is introduced into the NW thermomicrofluidics to release the EV-free miRNAs. Finally, the lysis buffer is introduced into the NW thermomicrofluidics to rupture the EVs, and EV miRNAs are obtained.

then, phosphate-buffered saline (PBS) was introduced into the NW thermomicrofluidics to remove the remaining sample from the channels. In the second step, specific temperatures were set for heating during PBS fluid delivery to release EV-free miRNAs preferentially. In the third step, lysis buffer was supplied to the NW thermomicrofluidics to rupture the EVs *in situ*, and EV miRNAs were obtained. These steps extracted miRNAs accompanied by information from inside or outside the EVs using a small sample volume and a short extraction time (35 min).

## Characterization of LNPs and interaction with NWs

For proof-of-concept validation, a model mixture was used to mimic miRNA sources from body fluids. This mixture consisted of EV-like lipid nanoparticles (LNPs) encapsulating synthesized miRNA miR-21 as the EV miRNAs, which were produced by an invasive LNP production device (iLiNP device),[19] and synthesized miRNA miR-155 as the EV-free miRNAs (Figure 2A). The cryogenic transmission electron microscopy (cryo-TEM) image shows that the miR-21-LNPs had a spherical shape and approximate size of 100 nm (Figure 2B). The size distributions show that the LNPs without and with miR-21 had mean sizes of 84 and 100 nm, respectively (Figure 2C), which were close to the appropriate mean EV sizes.[20] The mean zeta potentials of LNPs without and with miR-21 were −16.23 and −19.17 mV, respectively (Figure 2D), which were close to the zeta potential of EVs from biological samples.[21] An evaluation using Alexa-Fluor-488-modified miR-21 at the 5′ carbon of the sugar molecule instead of bare miR-21 for fluorescence measurement using nanoparticle flow cytometry confirmed encapsulation of miR-21-Alexa Fluor 488 (Figure 3A). The increase of the mean size, the decrease of the mean zeta potential, and the fluorescence confirmation of the LNPs after encapsulation of miR-21 highlighted that miR-21 was inside the LNPs. Removal of miR-21 not encapsulated in LNPs by dialysis treatment and subsequent addition of miR-155 produced the mixed sample of miR-21-LNPs and miR-155 for mimicking EV miRNA and EV-free miRNA sources from body fluids.

The NWs showed a high capture efficiency for both the individual introductions and the introduction of the mixture of miR-155 and miR-21-LNPs (Figure 3B). The individual solutions and the model mixture of miR-155 and miR-21-LNPs were introduced into the device according to the procedure for miRNA discrimination (Figure 1). The capture efficiency was calculated by using $(C_0 - C)/C_0$, where $C_0$ is the initial concentration of miRNAs and $C$ is the uncaptured concentration of miRNAs, quantified by quantitative PCR (qPCR). The capture efficiencies for the individual introductions of miR-155 and miR-21-LNPs were 99.81% and 80.83%, respectively. When the mixture was introduced as a competitive capture, miR-155 and miR-21-LNPs were captured on the device with a slight decrease in capture efficiency compared to the individual introductions; the capture efficiencies of miR-155 and miR-21-LNPs were 97.26% and 78.87%, respectively. After introducing miR-21-LNPs in PBS for capture and then removing the remaining sample from the channels using PBS, we found that miR-21-LNPs were on the NWs, as observed in our field emission scanning electron microscopy (FESEM) images (Figure 3C). These results confirmed that the NWs could capture both miRNAs and EV-like LNPs simultaneously and that the captured LNPs were not ruptured.

## Capture mechanism of EVs and EV-free miRNAs on NWs

To understand the capture mechanism of EV-free miRNAs on NWs, we confirmed the type of interaction between short-length miRNAs and NWs (poly(A)-NW) by analyzing spectral characteristics using Fourier transform infrared (FTIR) spectroscopy (Figures 4A and S1). Since the NW surfaces are known to be fully covered by a tightly bound water layer,[22] we expected the interaction of poly(A)-NWs to be hydrogen bonding. In the infrared (IR) spectrum of the poly(A) (s) (i.e., the solid state of poly(A)), the amine deformation vibration band, $\delta(NH_2)$, was observed at 1,646 $cm^{-1}$. In the spectrum of poly(A) dispersed in ultrapure water (poly(A) (l)), due to hydration, the peak of $\delta(NH_2)$ appeared at 1,650 $cm^{-1}$, which is a higher wavenumber than that of poly(A)

Please cite this article in press as: Chattrairat et al., Discrimination of extracellular miRNA sources for the identification of tumor-related functions based on nanowire thermofluidics, Device (2024), https://doi.org/10.1016/j.device.2024.100363



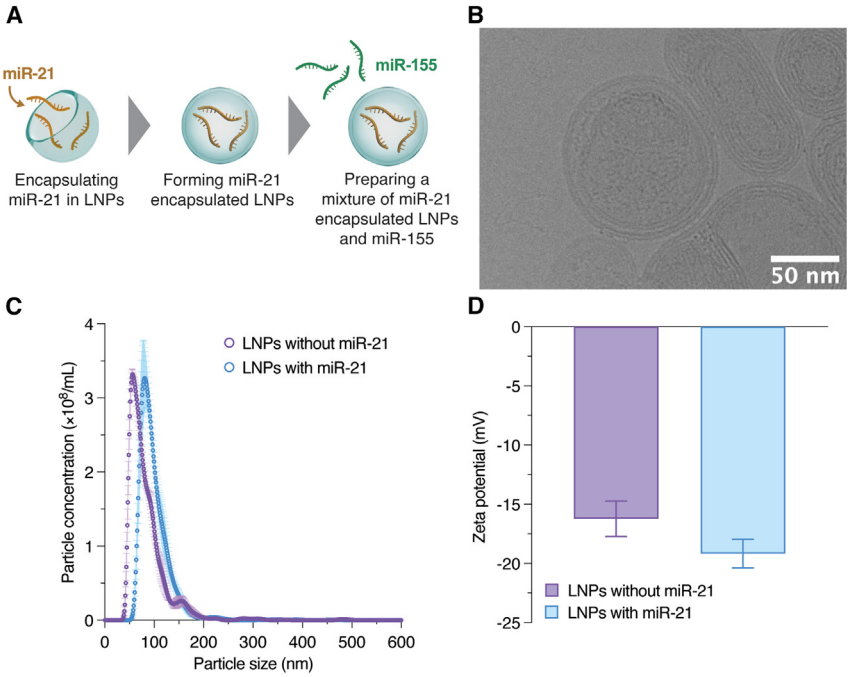


**Figure 2. Characterization of LNPs with and without miR-21**

(A) Schematic images describing encapsulation of miR-21 in LNPs and preparation of a mixture of miR-21-LNPs and miR-155.

(B) A close-up view of the cryo-TEM image of the miR-21-LNPs; scale bar, 50 nm.

(C) Size distributions of LNPs with and without miR-21. Data represent mean ± standard deviation ($n$ = 3 independent experiments).

(D) Zeta potential of LNPs with and without miR-21 in PBS of pH 7.4. Data represent mean ± standard deviation ($n$ = 3 independent experiments).

(s). As expected, the IR spectrum of poly(A) on NWs (poly(A)-NWs) had a higher $\delta(NH_2)$ wavenumber at 1,652 $cm^{-1}$, suggesting that hydrogen bonding occurred between the amine functional group of miRNAs and the water molecules on the NWs. Furthermore, the IR spectra of poly(U), poly(G), and poly(C) on NWs were also observed (Figure S1). The IR spectra of short-length miRNAs and NWs showed that hydrogen bonding between miRNAs and NWs occurred mainly at amine ($-NH_2$) and ketone (C=O) functional groups, depending on the molecular structure of the miRNAs.

We used FTIR to investigate the interaction between LNPs and NWs (Figure 4B). The IR spectra of the solid-state LNPs, i.e., LNPs (s), indicated that the LNPs interacted with NWs mainly through hydrogen bonding of the phosphate group. The LNPs (s) were obtained by a freeze-drying process and dispersed in ultrapure water as LNPs (l). Then, the LNPs (l) were dropped and simultaneously dried on the NWs to obtain LNPs-NWs. In the IR spectra of LNPs (s), two types of phosphate symmetric stretching vibration peaks appeared, one in the free state (1,091 $cm^{-1}$) and the other in the intermolecularly interacting state (1,055 $cm^{-1}$), suggesting that intermolecular association occurred in the frozen-solid phase. When LNPs (s) are redispersed in ultrapure water, the peaks from the free state and the intermolecularly interacting state disappeared in the spectrum of LNPs (l), and instead, another peak (1,080 $cm^{-1}$) due to hydration appeared. These results indicated that the peak position (1,062 $cm^{-1}$) in LNP-NWs was due to the hydrogen bonding between the phosphate group of the LNPs and the water molecules on the NWs; however, another peak remained around 1,100 $cm^{-1}$, indicating the coexistence of LNPs that appeared to be physically adsorbed on the NWs. In addition, the phosphate group peak of each lipid and the ZnO NWs also exhibited a lower wavenumber shift that supported the evidence of interaction by LNP-NWs (Figure S2). Using p-polarized multiple-angle incidence resolution spectrometry (pMAIRS), we determined that LNPs as a spherical shape interacted with NWs of random orientation because the intensity ratio of the in-plane band intensity divided by the out-plane band intensity is close to the intensity ratio of 1[23] (Figure 4C). On the other hand, the orientations of each lipid absorbed on NWs were different due to their interactions and chemical structures (Figures 4C and S2). Hence, these results confirmed that ZnO NWs captured intact LNPs through hydrogen bonding between the LNP phosphate groups and the water molecules on the ZnO NWs.

Molecular dynamics (MD) simulations were conducted to further analyze the capture mechanism, specifically, the hydrogen bonding observed between the captured molecules and the water molecules on the ZnO NWs, as revealed by the IR spectra. The IR spectra showed that the phosphate groups of 1,2-dioleoyl-*sn*-glycero-3-phospho-L-serine (DOPS) and 1,2-distearoyl-*sn*-glycero-3-phosphocholine (DSPC) in LNPs could interact with the NWs, and the amine groups of adenine and uracil in miRNAs could interact with the NWs. Due to the size and complexity of the molecules, the MD simulations could not be performed for LNPs, and the simulations were performed for miRNAs at 5-mers with shortened bases (Figures 4D, 4E, and S3). In the distribution of poly(A) and poly(U), miRNA peaks were observed near the second and third peaks of water, and no desorption was observed after adsorption on the ZnO surface during the simulation. In the distribution of poly(G) and poly(C), there were no miRNA peaks on the ZnO surface, and during the simulation, once adsorbed on the ZnO surface, poly(G) and poly(C) were quickly rereleased, and over time they were rarely adsorbed stably. The MD simulation results showed that ZnO was covered by a layer of water, that ZnO and miRNAs were not directly adsorbed, and that the strength of adsorption expressed by the number density distribution on the ZnO surface followed the order from strongest to weakest of poly(A), poly(U), poly(G), and poly(C).

## miRNA extraction for the model mixture

The miRNA source discrimination in NW thermomicrofluidics is based on the fact that thermal preferential release is possible due to differences in the interactions of EV-free miRNAs and

Please cite this article in press as: Chattrairat et al., Discrimination of extracellular miRNA sources for the identification of tumor-related functions based on nanowire thermofluidics, Device (2024), https://doi.org/10.1016/j.device.2024.100363





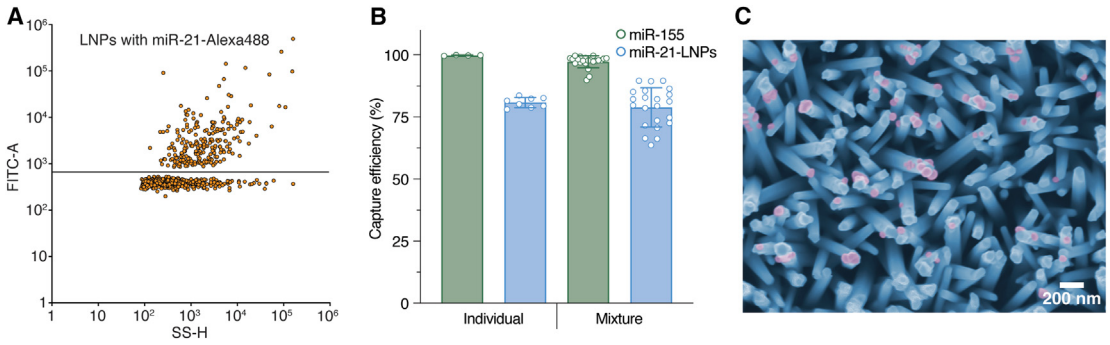


**Figure 3. Capture efficiency of miRNAs and LNPs on NWs**

(A) Nanoscale flow cytometry identifying LNPs with miR-21-Alexa 488.

(B) Capture efficiency of individual introduction of miR-155 (2.79 μM) and miR-21-LNPs (2.75 × $10^9$ particles/mL) and mixtures of miR-155 (1.91 μM) and miR-21-LNPs (1.02 × $10^9$ particles/mL). Data represent mean ± standard deviation ($n \geq 4$ independent experiments).

(C) FESEM image of miR-21-LNPs on ZnO nanowires; scale bar, 200 nm. The miR-21-LNPs and ZnO nanowires are highlighted in red and blue, respectively.

EVs with NWs. Considering the results that miR-155 bound to the NWs through the amine and ketone groups in miRNAs and miR-21-LNPs bound to the NWs through the phosphate groups in LNPs, it is likely that both miRNAs and LNPs have multi-point hydrogen bonding, which plays an important role in setting the strength of the interaction. Moreover, considering the number of bases in miRNAs (18–24 nucleotides in length) and the number of phosphate groups (50 mol %) in LNPs with a diameter of about 100 nm, it can be assumed that miRNAs have fewer binding sites and are more easily thermally released than LNPs. The release efficiencies of the individual introductions of miR-155 and miR-21-LNPs after supplying PBS during heating differ according to temperature (Figures 5A and 5B). These differences occurred because, with higher temperatures, a higher number of hydrogen bonds can be interrupted, leading to higher release efficiencies. Conversely, lower temperatures have the opposite effect. The release efficiency and miRNA recovery were calculated using $C_r/C_0$, where $C_r$ is released concentration after supplying PBS during heating or recovered concentration after supplying lysis buffer, and $C_0$ is initial concentration. At 95°C, the release efficiency of miR-21-LNPs was around 21%, while the release efficiency of miR-155 was up to 80%, indicating that miR-155 could be removed from the device by the thermal energy preferentially; we selected 95°C for running the subsequent experiments. A low flow rate of the PBS delivery during heating could considerably increase the release efficiency of miR-155, whereas the release efficiency of miR-21-LNPs was only slightly increased (Figure S4). These results suggested that the NW thermomicrofluidics preferentially released EV-free miRNAs from the mixture when PBS was supplied during heating, and subsequently it collected EV miRNAs after lysis buffer was supplied.

When comparing the miRNA concentration recovery between NW thermomicrofluidics and the UC method, we found that the NW thermomicrofluidics provided markedly greater miRNA recovery of both miR-155 and miR-21 under identical initial conditions (Figure 5C). The miRNAs were recovered from the NW thermomicrofluidics after supplying PBS during heating as miRNAs, released through the thermal process, and after supplying lysis buffer as lysate miRNAs. Among the miRNAs released through the thermal process after supplying PBS during heating, the recoveries of miR-155 and miR-21 were 64% and 33%, respectively, due to thermal release and rupture of the LNPs (Figures 5C and S5). Then, among the lysate miRNAs after supplying lysis buffer, miR-155 recovery was only 3%, while miR-21 recovery was as high as 63%; the contamination rate of miR-155 was less than 5%. Although the UC method could isolate and extract the miRNAs from the model mixture at the same volume and concentration as for the NW thermomicrofluidics, it obtained an extremely low recovery concentration for each miRNA. Moreover, the UC method was unable to separate only miR-21 from the model mixture, as a 30% contamination rate of miR-155 occurred. These results indicated that our NW thermomicrofluidics was practical for miRNA extraction and discrimination.

## miRNA source discrimination for ovarian cancer serum samples

We demonstrate the ability of the NW thermomicrofluidics to discriminate the sources of extracellular miRNAs for ovarian cancer serum samples as EV miRNAs and EV-free miRNAs (Figure 6). The application to ovarian cancer of miRNA diagnostics in serum is recognized as one of the most successful uses.[24] For lysate miRNAs, almost all of them are thought to be EV miRNAs because the contamination rate is less than 5%, but for miRNAs released through the thermal process, we can only conclude that there are many EV-free miRNAs, because the contamination rate of EV miRNAs is as high as 50%. The volcano plot shown in Figure 6A was constructed to analyze the miRNA expression by plotting differential miRNA expression values, i.e., $\log_2$(released miRNA/lysate miRNA), versus statistically significant values, i.e., $-\log_{10}(p$ value), calculated by the unpaired two-tailed t test. The volcano plot shows the statistically significant miRNAs, highlighted in orange and green for assigning lysate miRNAs and miRNAs released through the thermal process, respectively. We assigned 2 miRNAs as lysate miRNAs and 12 miRNAs as miRNAs released through the thermal process and matched each miRNA to its tumor-related functions (Table 1). As the contamination rate of miRNAs released through the thermal process after adding lysis buffer was less than 5%,

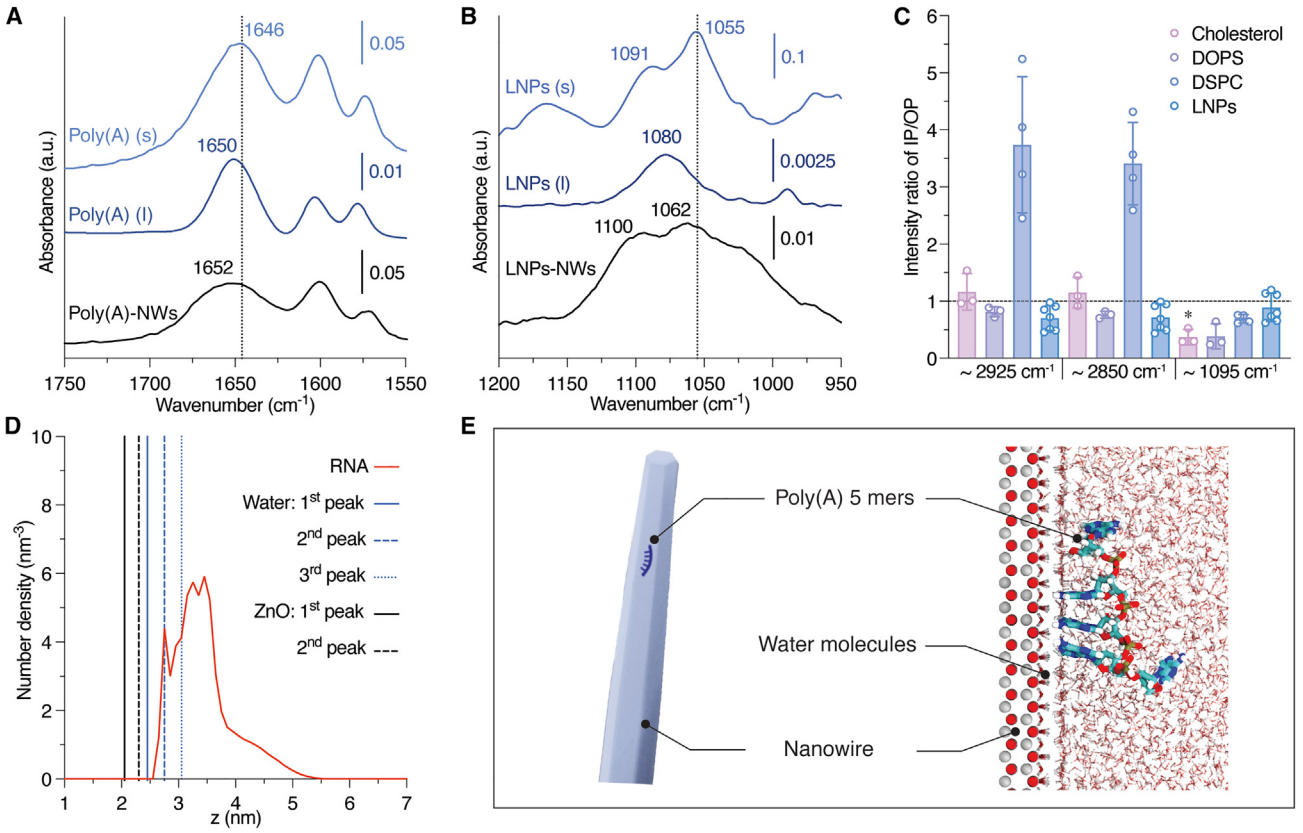


**Figure 4. Capture mechanism of miRNAs and LNPs on NWs**

(A) IR spectra of poly(A) (s), poly(A) (l), and poly(A)-NWs. The vertical dashed line indicates the wavenumber 1,646 $cm^{-1}$.

(B) IR spectra of LNPs (s), LNPs (l), and LNP-NWs. The vertical dashed line indicates the wavenumber 1,055 $cm^{-1}$.

(C) Intensity ratio of the in-plane (IP) band intensity to the out-plane (OP) band intensity in the pMAIRS spectra. The horizontal dashed line indicates the intensity ratio 1, which means the molecules are randomly oriented. The intensity ratio was calculated for the peaks of the $CH_2$ anti-symmetric (~2,925 $cm^{-1}$) and symmetric (~2,850 $cm^{-1}$) stretching vibration bands and the phosphate symmetric stretching vibration band (~1,095 $cm^{-1}$). *The C−O stretching vibration band (~1,057 $cm^{-1}$) was used for cholesterol. All the data represent the mean ± standard deviation ($n \geq 3$ independent experiments).

(D) MD simulation results for poly(A).

(E) A schematic image of poly(A) captured on a nanowire and a simulation image of poly(A) captured on nanowires. Atoms included in the images are carbon (cyan), nitrogen (blue), oxygen (red), hydrogen (white), phosphate (yellow), and zinc (gray).

we concluded that these two lysate miRNAs were EV miRNAs that matched oncogenic miRNAs.

The heatmap for the assigned 14 miRNAs showed that the oncogenesis miRNAs were preferentially present in the lysate miRNAs, whereas the tumor-suppressor miRNAs were present in the miRNAs released through the thermal process (Figure 6B). As mentioned above, the lysate miRNAs had a high probability of being EV miRNAs, while miRNAs released through the thermal process could be both EV miRNAs and EV-free miRNAs. To determine whether the tumor-suppressor miRNAs were EV miRNAs or EV-free miRNAs, we constructed a heatmap of the expression levels of the let-7 family, a well-known tumor-suppressor miRNA,[25] and the results showed that the expression of the let-7 family was mostly in the miRNAs released within the thermal process regions (green lines in Figure 6C). Furthermore, statistically significant 3.74- and 3.32-fold changes were observed in the expression levels of let-7i-5p and let-7g-5p, respectively (Figure 6D). These changes exceeded the contamination rate of EV miRNAs, thereby providing a high level of confidence that the miRNAs released through the thermal process were EV-free miRNAs. Moreover, if we consider that the thermal stability of EVs[26] (Figure S6) is higher than that of LNPs (Figure S5), the actual contamination level of EV miRNAs in miRNAs released through the thermal process might be lower. Including these assumptions, we concluded that the lysate miRNAs and the miRNAs released through the thermal process, which were extracted from serum of ovarian cancer patients, were EV miRNAs and EV-free miRNAs, respectively.

Although more trials and further downstream analyses are required for clear recognition of the miRNA sources, our statistical analysis demonstrated two miRNA sources, EV miRNAs and EV-free miRNAs, and revealed the correlation between miRNA source and tumor-related functions. The EVs pack various essential biological compounds, including miRNAs,[4] and they are involved in developing organ-specific metastasis; hence, we supposed that some miRNA functions could be related to

Please cite this article in press as: Chattrairat et al., Discrimination of extracellular miRNA sources for the identification of tumor-related functions based on nanowire thermofluidics, Device (2024), https://doi.org/10.1016/j.device.2024.100363





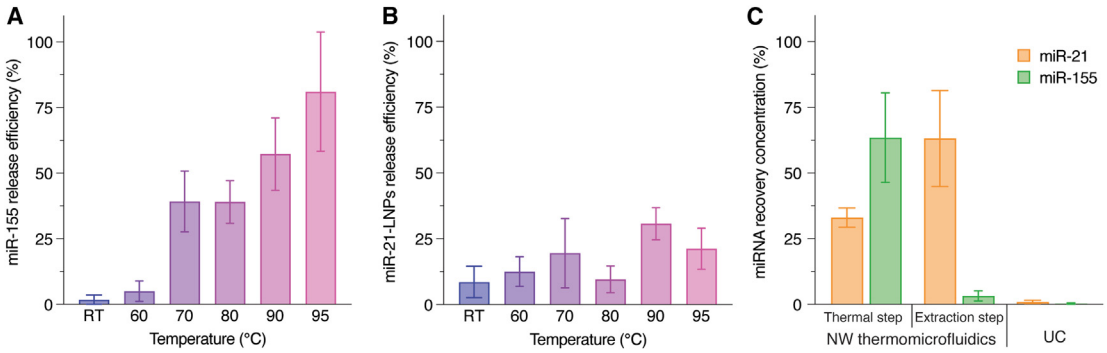


**Figure 5. miRNA extraction for the model mixture**

(A and B) Thermal release efficiency at different temperatures for individual introductions of (A) miR-155 and (B) miR-21-LNPs. Data represent mean ± standard deviation ($n \geq 3$ independent experiments).

(C) Recovery of miR-21 and miR-155 by NW thermomicrofluidics and ultracentrifugation (UC) from the mixture of miR-155 and miR-21-LNPs. For NW thermomicrofluidics, the thermal step showed the miRNA recovery after supplying PBS during heating, and the extraction step showed the miRNA recovery after supplying lysis buffer. After ultracentrifugation was performed, the miR-21 and miR-155 were obtained by supplying lysis buffer. Data represent mean ± standard deviation ($n \geq 3$ independent experiments).

their source[27] (Table 1). miR-21-5p and miR-30e-5p, assigned as EV miRNAs (Figure 6D), have been previously identified and reported as oncogenesis miRNAs promoting peritoneal metastasis.[28,29] In contrast, miR-29c-3p and miR-101-3p are examples of higher expression levels in EV-free miRNAs than in EV miRNAs (Figure 6D), and both have been reported to be tumor suppressors in ovarian cancer.[30,31] Some miRNAs assigned as EV-free miRNAs had different tumor-related functions, such as miR-99a-5p and miR-423-5p (Figure 6D and Table 1); further experiments and downstream miRNA pathway analyses are required to confirm each miRNA source. However, given the possibility that EV-free miRNAs also contain EV miRNAs and the function of the two miRNAs identified as EV miRNAs, it is likely that EV miRNAs are oncogenesis miRNAs and EV-free miRNAs are tumor-suppressor miRNAs. These results demonstrated that each miRNA had its own specific tumor-related function; therefore, the discrimination and extraction of miRNAs by our NW thermomicrofluidics could provide a better understanding of miRNA biogenesis, functions, and pathways.

## DISCUSSION

### Required volume and time for EV isolation and miRNA extraction

Unlike the widely used conventional UC method for EV analysis, NW thermomicrofluidics provides the capability to capture both EVs and EV-free miRNAs, then release EV-free miRNAs preferentially, and finally extract EV miRNAs from EVs, leading to discrimination of miRNA sources for further tumor-related miRNA analysis. Considering the features of required volume, time, and ability to collect miRNAs, the NW thermomicrofluidic device can provide high capture efficiency using a small sample volume with a short extraction time. As many efforts have been extended to develop the methodology for EV isolation and extraction in terms of, e.g., required volume and extraction time, we have summarized the required volume and time in various EV isolation and extraction methodologies for human serum or plasma (Table 2). The UC method could isolate and extract miRNA from human serum or plasma after lysis buffer is supplied; however, it requires a large sample volume and takes more than 180 min. Some emerging methodologies have been used for EV isolation and extraction: ExoQuick, size-exclusion columns, microfluidic devices, and polymer-based precipitation. However, each requires much larger sample volumes than our device, which needs only 50 μL of human serum and 35 min for both capturing EV and EV-free miRNA and extracting EV miRNA and EV-free miRNA. Our device provides the capability for extracellular miRNA source discrimination between EV miRNAs and EV-free miRNAs, which can pave the way for further downstream analyses and disease diagnoses and prognoses based on miRNA analysis. Our findings also revealed that oncogenesis miRNAs are favorably packed inside the EVs, and conversely, tumor-suppressor miRNAs are present outside the EVs.

It is worth noting that it is possible to divide a large amount of a single sample into two halves and use conventional methods to discriminate miRNAs. However, the final goal of human sample collection should be noninvasive sample collection, such as urine, sweat, saliva, and tears. Considering the volume of serum samples, we minimized the required volume of serum samples, as the sample collection was invasive. Therefore, we used only 50 μL for both extraction and discrimination of miRNAs. With a small amount of sample, our device was able to extract and discriminate the miRNAs, whereas the UC method obtained a very low miRNA recovery concentration (Figure 5C).

### Interaction of miRNAs and LNPs on NWs

Poly(A) was strongly adsorbed on the ZnO surface due to hydrogen bonding between the water strongly bound to the ZnO surface (water located at the first peak) and the amino group in the base, and at most, all five bases were adsorbed on the ZnO surface. In addition, poly(A) was also observed to form hydrogen bonds with the sugar alcohols and water on the ZnO surface (Figures 4A and 4E). Poly(U) did not adsorb all the bases as poly(A) did, but it had a structure in which three bases were

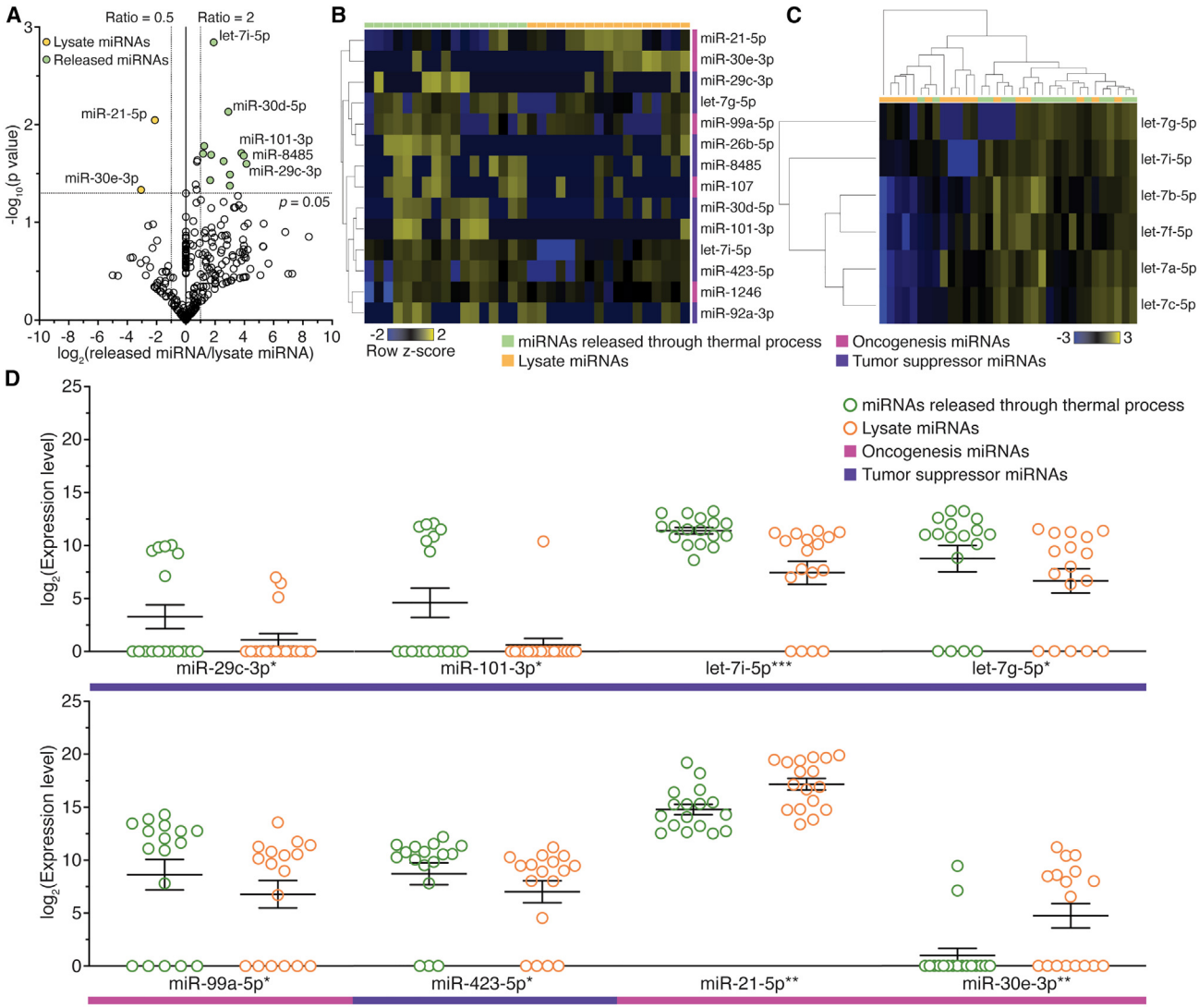


**Figure 6. miRNA discrimination and extraction using NW thermomicrofluidics for ovarian cancer serum samples ($n$ = 17): volcano plot, heatmaps, and miRNA expression levels**

(A) The volcano plot shows differential miRNA expression, i.e., the ratio of the averaged miRNA expression level of miRNA released through the thermal process to the lysate miRNA. Each point corresponds to a different miRNA type. The horizontal dashed line is the cut-off $p$ value of 0.05 and the vertical dashed lines are the cut-off differential miRNA expressions of 0.5 and 2.

(B) Heatmap showing the miRNAs in double filtering areas of the volcano plot. The miRNA information is also presented in Table 1.

(C) Heatmap showing the expression levels of the let-7 family.

(D) Presentation of some miRNA expression levels in (B) and (C). Data represent mean ± standard error of mean ($n$ = 17). The $p$ value was calculated by an unpaired two-tailed t test (*$p$ < 0.05, **$p$ < 0.01, ***$p$ < 0.005). In (B) and (C), green and orange highlight miRNAs released through the thermal process and lysate miRNAs, respectively. In (B), (C), and (D), pink and purple highlight oncogenesis and tumor-suppressor miRNAs, respectively.

simultaneously adsorbed on ZnO with N–H of the base acting as a hydrogen bond donor for a long time during the simulations (Figure S3A). Poly(C) and poly(G), like poly(A), adsorbed on the ZnO surface via sugar alcohols, phosphate groups, and amino groups, but the adsorption structure was more disordered than that of poly(A) and poly(U), and the adsorption state was not stable (Figures S3B and S3C). Considering the MD simulation results in light of the chemical structure, poly(A) has only a hydrogen bond donor (amino group) to the base and there is nothing to prevent hydrogen bonding; therefore, stable adsorption is possible. Poly(C) and poly(G) have not only donor amino groups but also acceptor carbonyl groups in the vicinity of the amino groups, so even if they adsorb onto the ZnO surface via amino groups, the structure is not stable due to electrostatic repulsion between the neighboring carbonyl groups and the ZnO surface, and the adsorption is not stable because the bases are on the surface. Poly(U) also has a carbonyl group, so its adsorption strength is not as strong as that of poly(A). However,

Please cite this article in press as: Chattrairat et al., Discrimination of extracellular miRNA sources for the identification of tumor-related functions based on nanowire thermofluidics, Device (2024), https://doi.org/10.1016/j.device.2024.100363





**Table 1. Potential ovarian tumor-related miRNAs identified by volcano plot analysis**

| Type of miRNA | Differential miRNA expression (released miRNAs/lysate miRNAs) | miRNA source | Tumor-related function | Reference |
|---|---|---|---|---|
| miR-29c-3p | 17.68 | released miRNA | suppressor | Xu et al.[30] |
| miR-8485 | 15.52 | released miRNA | suppressor | Li et al.[59] |
| miR-101-3p | 13.97 | released miRNA | suppressor | Guo et al.[31] |
| miR-92a-3p | 8.09 | released miRNA | suppressor | Liu et al.[60] |
| miR-26b-5p | 8.06 | released miRNA | suppressor | Zhu et al.[61] |
| miR-30d-5p | 7.47 | released miRNA | suppressor | Yu et al.[62] |
| miR-107 | 5.99 | released miRNA | suppressor | Liu et al.[63] |
| let-7i-5p | 3.74 | released miRNA | suppressor | Yang et al.[64] |
| let-7g-5p | 3.32 | released miRNA | suppressor | Biamonte et al.[65] |
| miR-99a-5p | 3.16 | released miRNA | oncogenesis | Yoshimura et al.[66] |
| miR-423-5p | 2.38 | released miRNA | suppressor | Du et al.[67] |
| miR-1246 | 2.27 | released miRNA | oncogenesis | Todeschini et al.[68] |
| miR-21-5p | 0.23 | lysate miRNA | oncogenesis | Cao et al.[69] |
| miR-30e-3p | 0.12 | lysate miRNA | oncogenesis | Lee et al.[29] |

The miRNAs located in the double filtering area of the volcano plot presented significant differential expression values. Following this analysis, the sources of these miRNAs were assigned, and their tumor-related functions were determined.

the N–H of the base of poly(U), which forms a hydrogen bond, has a symmetrical structure flanked by carbonyl groups, so it is not on the ZnO surface due to asymmetric electrostatic repulsion, like poly(C) and poly(G), and thus adsorption is possible. From these considerations, high A and U sequences are likely to dominate miRNA adsorption to ZnO.

Accordingly, the IR spectra of the interaction of miRNAs on NWs and their molecular structures also demonstrated a similar trend compared with the MD simulation (Figure S1). We found the strongest adsorption for poly(A) was by the interaction between the amine ($–NH_2$) functional groups and water molecules on the NWs. In addition, since poly(A) has only one adsorption moiety, the steric effect is nonsignificant.[32,33] Poly(U) can interact with the NWs via the ketone (C=O) functional group; poly(U) has a weaker interaction with water molecules than the amine ($–NH_2$) functional group, and the uracil structure is smaller than the adenine structure, leading to a weak interaction with the NWs. Poly(G) and poly(C), respectively, had the third and the fourth strongest adsorption because the interaction can occur in both ketone and amine functional groups, demonstrating a competitive interaction and steric effect.[32,33]

## Flow rate effect on release efficiency

We observed that the release efficiency of miR-155 decreased as the flow rate increased (Figure S4). To explain this finding, we considered two possibilities. First, the temperature did not reach 95°C. However, we believed that this possibility was low because we fabricated the device with feedback control to ensure that the temperature was maintained at the desired temperature. Moreover, we had two thermocouples above and below the substrate to ensure that the temperature reached the desired point. Second, the decrease of release efficiency of miR-155 with increasing flow rate was due to the heat capacity and contact time. With a high flow rate, the solution did not have enough time to release the miRNA from the NW surface. Conversely, with a low flow rate, the solution had enough time to store the heat and release the miRNA from the NW surface.

## Thermal stability of miRNAs, LNPs, and EVs

The thermal stability of miRNAs and LNPs is also important in miRNA source discrimination in NW thermomicrofluidics (Figure S5). The thermal stabilities of miR-21 and miR-21-LNPs were obtained by separately incubating the samples for 10 min at each of seven temperatures, from room temperature to 100°C. The concentration of miR-21 decreased by 0.3 ng/μL, approximately 11.5%, between room temperature and 100°C, and the concentration of miR-21-LNPs decreased by $1.54 \times 10^9$ particles/mL, approximately 40%, between room temperature and 100°C (Figures S5A and S5B). The size distribution of the concentration of miR-21-LNPs had a maximum at a particle diameter of about 100 nm, and their concentrations were lower at higher incubation temperatures, indicating that the particles were ruptured by incubation, with no change in LNP particle size due to incubation (Figure S5C). The decrease of the concentration of miR-21-LNPs at each temperature meant that miR-21 was released to the outside, leading to the increase of the concentration of miR-21 (Figure S5D). The miR-21 concentration after extraction was about 63% (Figure 5C), corresponding to the concentration of miR-21-LNPs remaining after thermal treatment, which was about 70% at 95°C (Figure S5B). EVs collected from the cell culture medium were found to be thermally stable enough to withstand temperatures as high as 100°C (Figure S6). These results implied that the miRNAs packed inside the EVs were protected against high temperature, and our device to discriminate between EV miRNAs and EV-free miRNAs via NW thermomicrofluidics was feasible.

## Release mechanism of unbound proteins and miRNA complexes

We considered the impact of unbound proteins on the collected EV miRNAs and EV-free miRNAs to be insignificant due to the

Please cite this article in press as: Chattrairat et al., Discrimination of extracellular miRNA sources for the identification of tumor-related functions based on nanowire thermofluidics, Device (2024), https://doi.org/10.1016/j.device.2024.100363



**Table 2. Required volumes and times in extraction methods of EVs and miRNAs**

| Extraction method | Required volume | Required time | Sample | Reference |
|---|---|---|---|---|
| Ultracentrifugation | ≥2,500 μL | ≥180 min | human serum | Otahal et al.[70] |
| Ultracentrifugation | 2,000 μL | ≥180 min | human plasma | Gutiérrez García et al.[71] |
| ExoQuick | ≥250 μL | ≥90 min | human serum, pleural fluid | Andreu et al.[72] |
| Size-exclusion columns | ≥900 μL | 25 min | platelet-free plasma | Gaspar et al.[73] |
| Microfluidic devices | 400 μL | 60 min | human serum | Kanwar et al.[74] |
| Polymer-based precipitation | ≥300 μL | ≥40 min (required further miRNA extraction) | human serum | Ozawa et al.[75] |
| NW thermomicrofluidics | 50 μL | 35 min | human serum | this study |

washing step. The washing step was used to eliminate the unbound proteins after introducing samples. In addition, we previously had verified that the ZnO NWs could effectively capture abundant EVs from biological samples such as cell culture media, urine, and serum.[12,16,17] The NW thermomicrofluidic device was designed to capture EVs and miRNAs from biological samples, eliminate unbound proteins through washing, and discriminate inside and outside extracellular miRNA sources in a single sample. We estimate that, through this method, the desorption of EVs is, at most, around 10%. Upon analysis of the composition of EVs,[10,34] it was evident that EV membranes constitute the majority of lipids and proteins. The biological relevance of the model mixture is limited by the relative simplicity of the artificial membranes compared to actual membranes, which comprise a considerably more diverse range of lipids and proteins. Within this group of substances comprising EVs, we contend that lipids have the simplest structure and exhibit the lowest binding strength to ZnO. In essence, as illustrated in Figure S4, the desorption percentage of LNPs, consisting solely of lipids, is approximately 10%, while we anticipate that the desorption percentage of more complex EVs is less than 10%.

Considering complexes of miRNAs with AGO or lipoproteins (e.g., HDLs and LDLs), having sizes ranging from around 5 to 25 nm, we concluded that the possibility of blocking the channel by these complexes was very low because the sizes of these complexes are much smaller than the channel size (Figure S7). Thus, we have determined two possibilities for capture and release of these complexes in our NW thermomicrofluidics. First, since the miRNAs are encapsulated in AGO or lipoproteins,[35,36] the AGO or lipoprotein complexes might be captured on NWs. However, if we consider the denaturation temperatures, around 50°C and 80°C for AGO and lipoprotein complexes, respectively,[37,38] we can conclude that AGO- and lipoprotein-complexed miRNAs were included in the miRNAs released through the thermal process at 95°C. Second, the AGO and lipoprotein complexes were not captured on NWs. The result for the second possibility means these complexes should flow through the channels and not include either miRNAs released through the thermal process or lysate miRNAs. Therefore, it is noteworthy that the miRNAs released through the thermal process represent four possible outcomes: (1) only EV-free miRNAs, (2) EV-free miRNAs mixed with EV miRNAs, (3) EV-free miRNAs mixed with AGO- or lipoprotein-complexed miRNAs, and (4) EV-free miRNAs mixed with EV miRNAs and AGO- or lipoprotein-complexed miRNAs. To gain a comprehensive understanding of the miRNAs released during the thermal process, further research and analysis are necessary. In summary, the AGO- and lipoprotein-complexed miRNAs were not in lysate miRNAs; therefore, we concluded that the lysate miRNAs were EV miRNAs.

Although conventional methods such as UC can extract the miRNAs from biological samples, the NW thermomicrofluidics is superior to the conventional methods due to its capability for high recovery of both EV miRNAs and EV-free miRNAs with a small sample volume and a short extraction time (Table 2). The NW thermomicrofluidics uses the advantage of the surface charge of the NWs to capture EVs with high efficiency as described in previous reports.[14,15] In the present study, we found that the ZnO NWs were covered by a layer of water and the phosphate group of the LNPs could interact with the NWs, and we assumed that the interaction between the NWs and the LNPs was mainly due to hydrogen bonding between the NW water layer and the LNP phosphate group. Considering also that the surface charge of the ZnO NWs is produced by the water layer on the NWs, this water layer is the key that led to the present miRNA discrimination. It is likely that the positively charged ZnO NWs attract negatively charged EVs and miRNAs to their surroundings via charge interactions, the water layer on ZnO NWs interacts with the phosphate groups of the EVs and amine groups of the miRNAs via hydrogen bonding, and the water layer on the ZnO NWs preferentially releases miRNAs due to fewer hydrogen bonding points than for EVs.

## Challenges and outlook

Despite these promising results, the current study has several limitations. First, for the thermal step, only EV-free miRNAs are expected to be released from the device; however, LNPs could be ruptured by thermal energy, leading to slight releases of EV miRNAs. Nevertheless, we evaluated the EV thermal stability, and the results showed that the EVs could withstand temperatures as high as 100°C. We attributed this to the components of EVs being more complex than those of LNPs; the EVs include, for example, membrane proteins, which could strengthen the lipid bilayer. Ideally, future studies should discriminate the miRNA sources with higher precision to obtain specific miRNAs and their functions.

While the NW thermomicrofluidics captured whole EVs from biological samples, specific EV capture by immunoaffinity can provide more specific miRNAs related to diseases rather than whole EV capture as reported previously.[39] However, specific

Please cite this article in press as: Chattrairat et al., Discrimination of extracellular miRNA sources for the identification of tumor-related functions based on nanowire thermofluidics, Device (2024), https://doi.org/10.1016/j.device.2024.100363





EV capture methods still require specific markers on EVs, such as a known specific membrane protein related to each disease. In contrast, without requiring specific markers, the NW thermomicrofluidics captured whole EVs and EV-free miRNAs and could provide miRNA information both inside and outside the EVs. To overcome a nonspecific EV capture, the surface modification on NWs with antibodies is expected to improve EV capture specificity.[40,41] Although the total number of ovarian cancer samples we assessed was enough to reveal the correlation between the miRNA sources and their tumor-related functions, better accuracy for classifying each tumor-related miRNA and its source should be obtained when a larger number of samples and diverse types of cancer are included and combined with machine learning. In this study, we only used serum for analyses. However, plasma is also commonly available from blood samples; sometimes, molecular profile results among them can differ.[42] When considering future applications, it is worthwhile to validate EV miRNAs in plasma, and for performance as biomarkers, further validation using a larger sample set is necessary.

## Conclusions

In summary, we demonstrated that NW thermomicrofluidics showed the capability to capture and discriminate EV miRNAs and EV-free miRNAs not only in the model mixture but also in actual ovarian cancer serum samples. The NW thermomicrofluidics is potentially an alternative method to investigate unclear miRNA sources. Instead of relying on capturing and analyzing only EV miRNAs for tumor-related information, our NW thermomicrofluidics is able to obtain more tumor-related information from both EV miRNAs and EV-free miRNAs. From the statistical analysis results, we concluded that oncogenesis miRNAs were favorably packed inside the EVs for cancer metastasis, and tumor-suppressor miRNAs were present outside the EVs. Moreover, our NW thermomicrofluidics required a small sample volume and a short time for discrimination and extraction of miRNAs. We demonstrated that there were two main miRNA sources in ovarian cancer serum, and this finding will pave the way for further downstream analysis based on miRNA research studies. Since NW thermomicrofluidics allows users to effectively discriminate and extract miRNAs, it will offer an opportunity to develop miRNA analytical systems for miRNA-based early diagnosis and prognosis with high precision and accuracy.

## EXPERIMENTAL PROCEDURES

### Resource availability

#### *Lead contact*

Further information and requests for resources should be directed to and will be fulfilled by the lead contact, Takao Yasui (yasuit@bio.titech.ac.jp).

#### *Materials availability*

This study did not generate new unique reagents.

#### *Data and code availability*

The datasets supporting the current study have not been deposited in a public repository but are available for research purposes from the lead contact author on request.

### Ethical approval and consent

The present study was approved and monitored by the ethics committee of Nagoya University Hospital (approval no. 2017-0497), and we obtained written informed consent from all patients who provided samples.

### Ovarian cancer serum collection

Blood samples were obtained from consenting patients with ovarian cancer who underwent surgery to remove tumors between 2020 and 2021 at Nagoya University Hospital. Blood samples were collected 1 day before the surgery date to exclude potential effects of anesthesia. The serum was isolated from whole blood immediately and stored at −80°C until further use. The patient cancer subtypes were pathologically diagnosed as given in Table S1.

### LNP and miR-21-LNP formation

LNPs were produced by the iLiNP device as described in the literature.[43] There were two inlets: aqueous solution and lipid inlets. For the aqueous solution inlet, 25 mM acetic buffer (pH 4.0) was prepared. For the lipid inlet, a 5 mM solution having a ratio of 10:45:45 mol % was prepared in ethanol:methanol of 8:2 for DOPS:DSPC:cholesterol (Chol) (Avanti Polar Lipid). The flow rates at the lipid and aqueous solution inlets were 166 and 332 μL/min, respectively. After LNP formation, a Spectra/Por 4 dialysis membrane (Repligen) was applied to remove contaminants using PBS (pH 7.4) at 4°C overnight. The LNPs were stored at 4°C until used in the next experiments. The miR-21-LNPs were also produced using the iLiNP device. For introduction via the lipid inlet, DOPS, DSPC, and Chol were prepared under the same liposome formation conditions. For introduction via the aqueous solution inlet, 13.4 mM $CaCl_2$ (Wako Pure Chemical Industries) and 70 μg/mL miR-21-5p (UAGCUUAUCAGACUGAUGUUGA) were prepared in 10 mM Tris (pH 8.0) (Nippon Gene). The flow rate was the same as for the liposome formation. Then, contaminants and remaining chemical substances were eliminated using the dialysis membrane in combination with PBS (pH 7.4) at 4°C overnight. The miR-21-LNPs were stored at 4°C before use.

### Characterization of LNPs

After the LNPs were produced, their concentration and size were analyzed using a nanoparticle tracking analysis (NTA) instrument (NanoSight LM10 HS; Malvern Panalytical). Video data were collected five times for a 60 s period each time. Camera level and detection threshold were set to 13 and 5, respectively. NanoSight NTA 3.2 software was used for data analysis. Zeta potentials of LNPs with and without miR-21 were measured using a commercial apparatus (zeta potential and particle size analyzer ELSZ-2000; Otsuka Electronics). The encapsulation of miR-21 was confirmed with a nanoparticle flow cytometer (model U30; NanoFCM) by plotting side-scatter height (SS-H) versus fluorescence intensity of fluorescein isothiocyanate (FITC). The threshold for the positive area was set to detect the miR-21-Alexa Fluor 488 (Figure 3A).

### Cryo-TEM measurement

A 3 μL aliquot of the prepared liposome solution was applied to a glow-discharged Quantifoil R1.2/1.3 200 mesh Cu grid (Quantifoil Micro Tools), which was then blotted for 3 s and plunge-frozen into liquid ethane using the Vitrobot Mark IV (Thermo Fisher Scientific). The liposome samples in the frozen-hydrated state were observed under cryogenic conditions with a CRYO ARM 300 II transmission electron microscope (JEOL) operated at 300 kV accelerating voltage. Images were recorded with a K3 direct electron detector (Gatan) at the nominal magnification of 60,000× using the SerialEM software.[44]

### NW fabrication and characterization

An S1112 micro glass slide (Matsunami Glass Industry) was used as a ZnO NW substrate. First, the substrate was cleaned with piranha solution, a mixed solution (1:4) of $H_2O_2$ (Wako Pure Chemical Industries) and $H_2SO_4$ (Wako Pure Chemical Industries), at 180°C for 2 h. Then, the substrate was cleaned using ultrapure water and dried with nitrogen gas. Photoresist (OFPR8600LB; Tokyo Ohka Kogyo) was coated on the substrate using the MS-A100 spin coater (Mikasa) at 500 rpm for 10 s and then at 1,500 rpm for 120 s. Next, the coated substrate was baked on a hot plate at 120°C for 10 min and then exposed through a microchannel photomask to UV radiation of 200 mJ/$cm^2$. After that, the substrate was developed with NMD-3 2.38% (Tokyo Ohko Kogyo) until the pattern appeared. The ZnO NW pattern length and width were 19 and 2.5 mm, respectively. We used a radio-frequency sputter (SVC-700RFII type I; Sanyu Electron) to deposit a ZnO layer on the patterned substrate before growing the ZnO NWs. The ZnO NWs were grown by the hydrothermal method at 95°C for

3 h using 50 mL of growth solution containing 50 mM zinc nitrate hexahydrate ($Zn(NO_3)_2 \cdot 6H_2O$; Thermo Fisher Scientific) and 50 mM hexamethylenetetramine (HMTA, $C_6H_{12}N_4$; Wako Pure Chemical Industries). Then, the patterned NW substrate was cleaned with acetone to remove the remaining photoresist. After that, it was rinsed with ultrapure water and dried by blowing nitrogen gas. The morphology of the ZnO NWs and LNPs on the NWs was characterized with the FESEM SUPRA 40VP (Carl Zeiss AG).

### NW thermomicrofluidic device fabrication

The NW thermomicrofluidic device was fabricated by bonding the patterned NW substrate and a herringbone-structured polydimethylsiloxane (PDMS) substrate. The herringbone-structured PDMS substrate had a microchannel (width, 2.5 mm; length, 19 mm; and height, 50 μm) with a 12-μm-high herringbone structure (Figure S7).[18] The PDMS substrate was prepared by mixing PDMS (Dow Corning Toray) and curing agent (Dow Corning Toray) in a ratio of 10:1. Then, the mixed solution was poured on the herringbone structure mold and kept in a vacuum chamber for approximately 1 h to eliminate any air bubbles. Curing was performed at 80°C for 2 h. After curing, the herringbone-structured PDMS substrate was obtained by cutting and removing it from the mold. The surface of the patterned NW substrate and the herringbone-structured PDMS substrate were treated using a SEDE-PFA soft etching device (Meiwafosis) and then bonded together. This bonded device was heated at 180°C for 3 min for strong bonding. Next, the herringbone-structured PDMS was connected to PEEK tubes (0.5 mm [outside diameter], 0.26 mm [inside diameter]; length, 10 cm; Institute of Microchemical Technology) for an inlet and outlet. When performing discrimination and extraction of miRNAs, the NW microfluidic device was set in the Peltier temperature controller to heat the NW thermomicrofluidics substrate.

### Discrimination and extraction of miRNA by NW thermomicrofluidics and UC

The model mixture of miR-155-3p (CUCCUACAUAUUAGCAUUAACA) and miR-21-LNPs at a volume of 50 μL was discriminated by both the NW thermomicrofluidics and the UC method. For the NW thermomicrofluidics, the samples were introduced and captured with a flow rate of 5 μL/min and then washed using 50 μL PBS (pH 7.4) with a flow rate of 10 μL/min. Subsequently, the thermal step was carried out by supplying 50 μL PBS (pH 7.4) at a flow rate of 5 μL/min during heating at 95°C. Finally, the extraction step was carried out using 50 μL lysis buffer (1% Triton X-100; Nacalai Tesque) in PBS (pH 7.4) at a flow rate of 5 μL/min. The miRNA concentration was then measured for each step using a reverse transcription (RT)-qPCR after purification with a microRNA Extractor SP kit (Fujifilm Wako Chemicals). The RT-qPCR was carried out using the Applied Biosystems TaqMan small RNA assays (Thermo Fisher Scientific) and the QuantStudio 3 real-time PCR system (Thermo Fisher Scientific). For the UC method, the samples were ultracentrifuged at 110,000 × *g* for 80 min at 4°C. Subsequently, the supernatant was discarded and PBS (pH 7.4) was added, before ultracentrifuging again under the same conditions as stated previously. Finally, the supernatant was discarded, and 1% Triton X-100 in PBS (pH 7.4) was added to rupture the LNPs. The solution was collected and purified with the microRNA Extractor SP kit. Then, the miRNA concentrations were measured using RT-qPCR.

### Thermal stability of miRNAs, LNPs, and EVs

To measure the thermal stability of LNPs, we measured the miR-21-LNPs and miR-21 concentrations by using NTA and RT-qPCR, respectively, before and after sample incubation at different temperatures (Figure S4). The EVs were derived from MDA-MB-231 cells. Dulbecco's modified Eagle's medium (DMEM, Thermo Fisher Scientific) with 10% fetal bovine serum (FBS; System Biosciences) containing 1% penicillin-streptomycin (PS; Thermo Fisher Scientific) without FBS was used to culture the cells for 48 h. The medium was changed to the advanced DMEM (Thermo Fisher Scientific) before collecting EVs. In each passage, $3 \times 10^6$ cells were seeded into 15 mL of cell medium in a T75 culturing flask (Iwaki) and cultured in a $CO_2$ incubator MCO-5AC (UV) (Sanyo Electric) at 37°C and in 5% $CO_2$ atmosphere. The cell culture medium was collected and centrifuged (10 min, 4°C, 300 × *g*), and the supernatant was collected and further centrifuged (10 min, 4°C, 2,000 × *g*). Then, the medium was filtered through a 0.22 μm filter (Merck Millipore). Next, the filtered medium was ultracentrifuged (80 min, 4°C, 110,000 × *g*). After discarding the supernatant, 6 mL of 0.22 μm filtered PBS (Thermo Fisher Scientific) was added to wash the collected EVs, followed by ultracentrifuging again (80 min, 4°C, 110,000 × *g*). After discarding the supernatant, 1 mL of 0.22 μm filtered PBS was added to collect the EVs that were then stored at 4°C. The EV concentrations before and after incubation were measured at different temperatures for 10 min each (Figure S5).

### IR spectra and the pMAIRS technique for the miRNA-NW and LNP-NW interactions

The IR spectra were measured with a Nicolet iS50 FTIR spectrometer (Thermo Fisher Scientific). The LNPs (s) were prepared by a freeze-drying process. LNPs (l) were prepared by redispersing LNPs (s) in ultrapure water. The miRNAs (s) (poly(A), poly(U), poly(G), and poly(C)) (Integrated DNA Technologies) were purchased and miRNAs (l) were prepared by dispersing miRNAs (s) in ultrapure water. IR spectra of LNPs (s), LNPs (l), miRNAs (s), and miRNAs (l) were measured using the attenuated total reflection (ATR) technique.[45] To observe the miRNA-NW and LNP-NW interactions, miRNAs (l) and LNPs (l) were dropped onto ZnO NWs grown on a double-polished silicon substrate. Finally, the substrate was allowed to dry at room temperature. Notably, for observing IR spectra, membrane dialysis of the LNPs was done with ultrapure water because, when the PBS was allowed to dry up, a salt stain formed on the substrate, which could interfere with the IR spectrum measurements. The sample preparation for the pMAIRS measurement was identical to that for ordinary IR spectrum measurements. The measurements were performed with the angle set (from 9° to 44° in 5° steps) using the p-polarized IR ray.[46–48]

### Peltier temperature controller fabrication

The heater for the NW thermomicrofluidics was composed of a Peltier PCR PTC40W temperature controller and thermocouple sensors (all manufactured by Axisnet). The thermocouple sensors were fixed onto the Peltier element and on the device substrate. The controller maintained the temperature at 25°C to 120°C with an accuracy of ±0.1°C. The locations where temperature was measured were above and below the NW microfluidic substrate.

### miRNA analysis by next-generation sequencing

The ovarian cancer serum samples with a volume of 50 μL were prepared using the same method as the model mixture. After ovarian cancer serum samples were collected for each step, the samples were purified using an miRNA purification kit (Norgen; Biotek). Then, the purified samples were treated with the NEBNext multiplex small RNA library prep set (New England Biolabs Japan) according to the manufacturer's instructions. Finally, miRNA types were analyzed using a next-generation sequencing instrument (NextSeq 550; Illumina). Then, raw files were trimmed and mapped to the miRbase 21 database, allowing up to two mismatches, using the CLC Genomics Workbench version 9.5.3 program (Qiagen). To analyze the volcano plot, we established a double filtering method to select miRNAs based on the following criteria: (1) $|\log_2(\text{released miRNA/lysate miRNA})| > 1$ and (2) $-\log_{10}(p \text{ value}) > 1.33$.[49] This double filtering method confirmed that the selected miRNAs were reliable because of a large-fold change and statistically significant test result. Thus, the miRNAs were divided into two groups: released miRNAs and lysate miRNAs. The criteria for assigning the source of miRNAs as EV miRNAs or EV-free miRNAs were set by $\log_2(\text{released miRNA/lysate miRNA}) < -1$ and $\log_2(\text{released miRNA/lysate miRNA}) > 1$, respectively. To generate a heatmap, we used the heatmap.2 function of the gplots package (v.3.0.1) given in the R software (v.4.0.3).

### Materials and methods for simulations

All MD simulations were performed using the GROMACS 2021.5 package.[50] The CHARMM36 force field[51,52] with the TIP3P model[53] was adopted for RNA and water molecules. The parameters of Zn and O from a previous study were employed.[54] We built a planar ZnO surface as a model of the ZnO NW. The $(10\,\bar{1}\,0)$ plane of the surface was exposed to a water slab with a thickness of about 4 nm. We prepared four types of 5-mer single-stranded RNA (ssRNA) molecules, namely, poly(A), poly(G), poly(C), and poly(U), and put them at approximately 2 nm away from the surface in the initial configuration. The periodic boundary condition was applied in the x and y directions. For the z

direction, we set a repulsive wall potential to limit the evaporation of water molecules. Temperature was controlled to be 300 K by the velocity rescaling method.[55] Electrostatic interaction was calculated using the two-dimensional particle mesh Ewald method.[56] The cut-off length of Lenard-Jones interactions was set to 1.2 nm with a force switching distance of 1.0 nm. The water geometries were kept constant by employing the SETTLE algorithm.[57] All bonds involving hydrogen atoms were constrained using the LINCS algorithm.[58] The simulation time step was set to 1 fs. Energy minimization with the steepest descent algorithm was conducted for all target systems to prevent unstable structures in the initial configurations. After that, we performed 50 ns MD simulations to equilibrate the systems in the NVT ensemble. Further 200 ns MD simulations were carried out as production runs for analyses. The MD trajectories saved every 1 ps were used to calculate the number density distributions of each molecule.

## SUPPLEMENTAL INFORMATION

Supplemental information can be found online at https://doi.org/10.1016/j.device.2024.100363.

## ACKNOWLEDGMENTS

This research was supported by the Japan Science and Technology Agency (JST) PRESTO (JPMJPR19H9), the New Energy and Industrial Technology Development Organization (NEDO) (JPNP20004), the JSPS Grant-in-Aid for Scientific Research (B) (21H01960), the Japan Agency for Medical Research and Development (AMED) (JP21he2302007), the Moonshot Research and Development Program (grant nos. 22zf0127004s0902 and JP22zf0127009) from the AMED, the Fusion Oriented Research for Disruptive Science and Technology (FOREST; JPMJFR204J) from the Japan Science and Technology Agency (JST), JST AIP Acceleration Research (JPMJCR23U1), the Takedarika Award for Young Researcher, and the RIKEN Junior Research Associate Program. Additional support was provided by the Platform Project for Supporting Drug Discovery and Life Science Research (Basis for Supporting Innovative Drug Discovery and Life Science Research [BINDS]) from AMED under grant no. JP22ama121038 (support no. 4008) and the Cooperative Research Program of the "Network Joint Research Center for Materials and Devices." Calculations were performed at the facilities of the Research Center for Computational Science, Okazaki (project 23-IMS-C095) and the Institute for Solid State Physics and the University of Tokyo. For their valuable discussions, we especially thank Dr. H. Yukawa, Dr. D. Onoshima, Dr. T. Shimada, and Dr. A. Arima.

## AUTHOR CONTRIBUTIONS

K.C. contributed to methodology, formal analysis, investigation, visualization, writing the original draft, and revising and editing. M.Z. and M.I. contributed to methodology. A.Y., K.Y., M.K., and H.K. contributed to sample preparation and sequence analysis. T.H. contributed to IR data analysis. M.M., A.N., and M.T. contributed to methodology and analysis. T. Yokoyama and Y.T. contributed to cryo-TEM observation. Y.M. and W.S. contributed to simulation analysis. K.N. and T. Yanagida contributed to data analysis. Y.B. contributed to conceptualization, funding acquisition, project administration, and supervision. T. Yasui contributed to conceptualization, funding acquisition, methodology, project administration, supervision, and revising and editing.

## DECLARATION OF INTERESTS

The authors declare no competing interests.

Received: November 13, 2023
Revised: November 14, 2023
Accepted: March 26, 2024
Published: April 22, 2024

## REFERENCES

1. Schee, K., Boye, K., Abrahamsen, T.W., Fodstad, Ø., and Flatmark, K. (2012). Clinical relevance of microRNA miR-21, miR-31, miR-92a, miR-101, miR-106a and miR-145 in colorectal cancer. BMC Cancer *12*, 505. https://doi.org/10.1186/1471-2407-12-505.
2. Lewis, B.P., Burge, C.B., and Bartel, D.P. (2005). Conserved seed pairing, often flanked by adenosines, indicates that thousands of human genes are microRNA targets. Cell *120*, 15–20. https://doi.org/10.1016/j.cell.2004.12.035.
3. Lawrie, C.H., Gal, S., Dunlop, H.M., Pushkaran, B., Liggins, A.P., Pulford, K., Banham, A.H., Pezzella, F., Boultwood, J., Wainscoat, J.S., et al. (2008). Detection of elevated levels of tumour-associated microRNAs in serum of patients with diffuse large B-cell lymphoma. Br. J. Haematol. *141*, 672–675. https://doi.org/10.1111/j.1365-2141.2008.07077.x.
4. Zhang, J., Li, S., Li, L., Li, M., Guo, C., Yao, J., and Mi, S. (2015). Exosome and exosomal microRNA: trafficking, sorting, and function. Cancer Genomics Proteomics *13*, 17–24. https://doi.org/10.1016/j.gpb.2015.02.001.
5. van Niel, G., D'Angelo, G., and Raposo, G. (2018). Shedding light on the cell biology of extracellular vesicles. Nat. Rev. Mol. Cell Biol. *19*, 213–228. https://doi.org/10.1038/nrm.2017.125.
6. Turchinovich, A., Tonevitsky, A.G., and Burwinkel, B. (2016). Extracellular miRNA: a collision of two paradigms. Trends Biochem. Sci. *41*, 883–892. https://doi.org/10.1016/j.tibs.2016.08.004.
7. Arroyo, J.D., Chevillet, J.R., Kroh, E.M., Ruf, I.K., Pritchard, C.C., Gibson, D.F., Mitchell, P.S., Bennett, C.F., Pogosova-Agadjanyan, E.L., Stirewalt, D.L., et al. (2011). Argonaute2 complexes carry a population of circulating microRNAs independent of vesicles in human plasma. Proc. Natl. Acad. Sci. USA *108*, 5003–5008. https://doi.org/10.1073/pnas.1019055108.
8. Turchinovich, A., Weiz, L., Langheinz, A., and Burwinkel, B. (2011). Characterization of extracellular circulating microRNA. Nucleic Acids Res. *39*, 7223–7233. https://doi.org/10.1093/nar/gkr254.
9. Michell, D.L., and Vickers, K.C. (2016). Lipoprotein carriers of microRNAs. Biochim. Biophys. Acta *1861*, 2069–2074. https://doi.org/10.1016/j.bbalip.2016.01.011.
10. Jeppesen, D.K., Fenix, A.M., Franklin, J.L., Higginbotham, J.N., Zhang, Q., Zimmerman, L.J., Liebler, D.C., Ping, J., Liu, Q., Evans, R., et al. (2019). Reassessment of exosome composition. Cell *177*, 428–445.e18. https://doi.org/10.1016/j.cell.2019.02.029.
11. Turchinovich, A., and Burwinkel, B. (2012). Distinct AGO1 and AGO2 associated miRNA profiles in human cells and blood plasma. RNA Biol. *9*, 1066–1075. https://doi.org/10.4161/rna.21083.
12. Yasui, T., Yanagida, T., Ito, S., Konakade, Y., Takeshita, D., Naganawa, T., Nagashima, K., Shimada, T., Kaji, N., Nakamura, Y., et al. (2017). Unveiling massive numbers of cancer-related urinary-microRNA candidates via nanowires. Sci. Adv. *3*, e1701133. https://doi.org/10.1126/sciadv.1701133.
13. Kitano, Y., Aoki, K., Ohka, F., Yamazaki, S., Motomura, K., Tanahashi, K., Hirano, M., Naganawa, T., Iida, M., Shiraki, Y., et al. (2021). Urinary microRNA-based diagnostic model for central nervous system tumors using nanowire scaffolds. ACS Appl. Mater. Interfaces *13*, 17316–17329. https://doi.org/10.1021/acsami.1c01754.
14. Paisrisarn, P., Yasui, T., Zhu, Z., Klamchuen, A., Kasamechonchung, P., Wutikhun, T., Yordsri, V., and Baba, Y. (2022). Tailoring ZnO nanowire crystallinity and morphology for label-free capturing of extracellular vesicles. Nanoscale *14*, 4484–4494. https://doi.org/10.1039/d1nr07237d.
15. Yasui, T., Paisrisarn, P., Yanagida, T., Konakade, Y., Nakamura, Y., Nagashima, K., Musa, M., Thiodorus, I.A., Takahashi, H., Naganawa, T., et al. (2021). Molecular profiling of extracellular vesicles via charge-based capture using oxide nanowire microfluidics. Biosens. Bioelectron. *194*, 113589. https://doi.org/10.1016/j.bios.2021.113589.
16. Chattrairat, K., Yasui, T., Suzuki, S., Natsume, A., Nagashima, K., Iida, M., Zhang, M., Shimada, T., Kato, A., Aoki, K., et al. (2023). All-in-one nanowire

assay system for capture and analysis of extracellular vesicles from an ex vivo brain tumor model. ACS Nano *17*, 2235–2244. https://doi.org/10.1021/acsnano.2c08526.

17. Yokoi, A., Ukai, M., Yasui, T., Inokuma, Y., Hyeon-Deuk, K., Matsuzaki, J., Yoshida, K., Kitagawa, M., Chattrairat, K., Iida, M., et al. (2023). Identifying high-grade serous ovarian carcinoma specific extracellular vesicles by polyketone-coated nanowires. Sci. Adv. *9*, eade6958. https://doi.org/10.1126/sciadv.ade6958.
18. Stroock, A.D., Dertinger, S.K.W., Ajdari, A., Mezić, I., Stone, H.A., and Whitesides, G.M. (2002). Chaotic mixer for microchannels. Science *295*, 647–651. https://doi.org/10.1126/science.1066238.
19. Kimura, N., Maeki, M., Ishida, A., Tani, H., and Tokeshi, M. (2021). One-Step production using a microfluidic device of highly biocompatible size-controlled noncationic exosome-like nanoparticles for RNA delivery. ACS Appl. Bio Mater. *4*, 1783–1793. https://doi.org/10.1021/acsabm.0c01519.
20. Arraud, N., Linares, R., Tan, S., Gounou, C., Pasquet, J.M., Mornet, S., and Brisson, A.R. (2014). Extracellular vesicles from blood plasma: determination of their morphology, size, phenotype and concentration. J. Thromb. Haemostasis *12*, 614–627. https://doi.org/10.1111/jth.12554.
21. Midekessa, G., Godakumara, K., Ord, J., Viil, J., Lättekivi, F., Dissanayake, K., Kopanchuk, S., Rinken, A., Andronowska, A., Bhattacharjee, S., et al. (2020). Zeta potential of extracellular vesicles: toward understanding the attributes that determine colloidal stability. ACS Omega *5*, 16701–16710. https://doi.org/10.1021/acsomega.0c01582.
22. Takahashi, H., Yasui, T., Hirano, M., Shinjo, K., Miyazaki, Y., Shinoda, W., Hasegawa, T., Natsume, A., Kitano, Y., Ida, M., et al. (2023). Mutation detection of urinary cell-free DNA via catch-and-release isolation on nanowires for liquid biopsy. Biosens. Bioelectron. *234*, 115318. https://doi.org/10.1016/j.bios.2023.115318.
23. Shioya, N., Fujiwara, R., Tomita, K., Shimoaka, T., and Hasegawa, T. (2020). Simultaneous analysis of molecular orientation and quantity change of constituents in a thin film using pMAIRS. J. Phys. Chem. A *124*, 2714–2720. https://doi.org/10.1021/acs.jpca.0c00111.
24. Yokoi, A., Matsuzaki, J., Yamamoto, Y., Yoneoka, Y., Takahashi, K., Shimizu, H., Uehara, T., Ishikawa, M., Ikeda, S.I., Sonoda, T., et al. (2018). Integrated extracellular microRNA profiling for ovarian cancer screening. Nat. Commun. *9*, 4319. https://doi.org/10.1038/s41467-018-06434-4.
25. Tristán-Ramos, P., Rubio-Roldan, A., Peris, G., Sánchez, L., Amador-Cubero, S., Viollet, S., Cristofari, G., and Heras, S.R. (2020). The tumor suppressor microRNA let-7 inhibits human LINE-1 retrotransposition. Nat. Commun. *11*, 5712. https://doi.org/10.1038/s41467-020-19430-4.
26. Schulz, E., Karagianni, A., Koch, M., and Fuhrmann, G. (2020). Hot EVs - how temperature affects extracellular vesicles. Eur. J. Pharm. Biopharm. *146*, 55–63. https://doi.org/10.1016/j.ejpb.2019.11.010.
27. Urabe, F., Patil, K., Ramm, G.A., Ochiya, T., and Soekmadji, C. (2021). Extracellular vesicles in the development of organ-specific metastasis. J. Extracell. Vesicles *10*, e12125. https://doi.org/10.1002/jev2.12125.
28. Li, Q., Li, B., Li, Q., Wei, S., He, Z., Huang, X., Wang, L., Xia, Y., Xu, Z., Li, Z., et al. (2018). Exosomal miR-21-5p derived from gastric cancer promotes peritoneal metastasis via mesothelial-to-mesenchymal transition. Cell Death Dis. *9*, 854. https://doi.org/10.1038/s41419-018-0928-8.
29. Lee, H., Park, C.S., Deftereos, G., Morihara, J., Stern, J.E., Hawes, S.E., Swisher, E., Kiviat, N.B., and Feng, Q. (2012). MicroRNA expression in ovarian carcinoma and its correlation with clinicopathological features. World J. Surg. Oncol. *10*, 174. https://doi.org/10.1186/1477-7819-10-174.
30. Xu, H., Mao, H.L., Zhao, X.R., Li, Y., and Liu, P.S. (2020). MiR-29c-3p, a target miRNA of LINC01296, accelerates tumor malignancy: therapeutic potential of a LINC01296/miR-29c-3p axis in ovarian cancer. J. Ovarian Res. *13*, 31. https://doi.org/10.1186/s13048-020-00631-w.
31. Guo, F., Cogdell, D., Hu, L., Yang, D., Sood, A.K., Xue, F., and Zhang, W. (2014). MiR-101 suppresses the epithelial-to-mesenchymal transition by targeting ZEB1 and ZEB2 in ovarian carcinoma. Oncol. Rep. *31*, 2021–2028. https://doi.org/10.3892/or.2014.3106.
32. Pinter, B., Fievez, T., Bickelhaupt, F.M., Geerlings, P., and De Proft, F. (2012). On the origin of the steric effect. Phys. Chem. Chem. Phys. *14*, 9846–9854. https://doi.org/10.1039/c2cp41090g.
33. Wagner, J.P., and Schreiner, P.R. (2015). London dispersion in molecular chemistry–reconsidering steric effects. Angew. Chem., Int. Ed. Engl. *54*, 12274–12296. https://doi.org/10.1002/anie.201503476.
34. Hallal, S., Tűzesi, Á., Grau, G.E., Buckland, M.E., and Alexander, K.L. (2022). Understanding the extracellular vesicle surface for clinical molecular biology. J. Extracell. Vesicles *11*, e12260. https://doi.org/10.1002/jev2.12260.
35. Chi, S.W., Zang, J.B., Mele, A., and Darnell, R.B. (2009). Argonaute HITS-CLIP decodes microRNA-mRNA interaction maps. Nature *460*, 479–486. https://doi.org/10.1038/nature08170.
36. Ouimet, M., and Moore, K.J. (2013). A big role for small RNAs in HDL homeostasis. J. Lipid Res. *54*, 1161–1167. https://doi.org/10.1194/jlr.R036327.
37. Lisitskaya, L., Shin, Y., Agapov, A., Olina, A., Kropocheva, E., Ryazansky, S., Aravin, A.A., Esyunina, D., Murakami, K.S., and Kulbachinskiy, A. (2022). Programmable RNA targeting by bacterial Argonaute nucleases with unconventional guide binding and cleavage specificity. Nat. Commun. *13*, 4624. https://doi.org/10.1038/s41467-022-32079-5.
38. Gursky, O. (2015). Structural stability and functional remodeling of high-density lipoproteins. FEBS Lett. *589*, 2627–2639. https://doi.org/10.1016/j.febslet.2015.02.028.
39. Ostenfeld, M.S., Jensen, S.G., Jeppesen, D.K., Christensen, L.L., Thorsen, S.B., Stenvang, J., Hvam, M.L., Thomsen, A., Mouritzen, P., Rasmussen, M.H., et al. (2016). miRNA profiling of circulating EpCAM(+) extracellular vesicles: promising biomarkers of colorectal cancer. J. Extracell. Vesicles *5*, 31488. https://doi.org/10.3402/jev.v5.31488.
40. Zhao, W., Hu, J., Liu, J., Li, X., Sun, S., Luan, X., Zhao, Y., Wei, S., Li, M., Zhang, Q., and Huang, C. (2022). Si nanowire Bio-FET for electrical and label-free detection of cancer cell-derived exosomes. Microsyst. Nanoeng. *8*, 57. https://doi.org/10.1038/s41378-022-00387-x.
41. Shimada, T., Yasui, T., Yokoyama, A., Goda, T., Hara, M., Yanagida, T., Kaji, N., Kanai, M., Nagashima, K., Miyahara, Y., et al. (2018). Biomolecular recognition on nanowire surfaces modified by the self-assembled monolayer. Lab Chip *18*, 3225–3229. https://doi.org/10.1039/c8lc00438b.
42. Lucien, F., Gustafson, D., Lenassi, M., Li, B., Teske, J.J., Boilard, E., von Hohenberg, K.C., Falcón-Perez, J.M., Gualerzi, A., Reale, A., et al. (2023). MIBlood-EV: Minimal information to enhance the quality and reproducibility of blood extracellular vesicle research. J. Extracell. Vesicles *12*, e12385. https://doi.org/10.1002/jev2.12385.
43. Kimura, N., Maeki, M., Sato, Y., Note, Y., Ishida, A., Tani, H., Harashima, H., and Tokeshi, M. (2018). Development of the iLiNP device: fine tuning the lipid nanoparticle size within 10 nm for drug delivery. ACS Omega *3*, 5044–5051. https://doi.org/10.1021/acsomega.8b00341.
44. Mastronarde, D.N. (2005). Automated electron microscope tomography using robust prediction of specimen movements. J. Struct. Biol. *152*, 36–51. https://doi.org/10.1016/j.jsb.2005.07.007.
45. Hasegawa, T. (2017). Quantitative Infrared Spectroscopy for Understanding of a Condensed Matter, 1 Edition (Springer Tokyo). https://doi.org/10.1007/978-4-431-56493-5.
46. Hasegawa, T. (2002). A novel measurement technique of pure out-of-plane vibrational modes in thin films on a nonmetallic material with no polarizer. J. Phys. Chem. B *106*, 4112–4115. https://doi.org/10.1021/jp013751b.
47. Hasegawa, T. (2007). Advanced multiple-angle incidence resolution spectrometry for thin-layer analysis on a low-refractive-index substrate. Anal. Chem. *79*, 4385–4389. https://doi.org/10.1021/ac070676d.

48. Hasegawa, T., and Shioya, N. (2020). MAIRS: Innovation of Molecular Orientation Analysis in a Thin Film. Bull. Chem. Soc. Jpn. *93*, 1127–1138. https://doi.org/10.1246/bcsj.20200139.

49. Li, W. (2012). Volcano plots in analyzing differential expressions with mRNA microarrays. J. Bioinf. Comput. Biol. *10*, 1231003. https://doi.org/10.1142/S0219720012310038.

50. Abraham, M.J., Murtola, T., Schulz, R., Páll, S., Smith, J.C., Hess, B., and Lindahl, E. (2015). GROMACS: high performance molecular simulations through multi-level parallelism from laptops to supercomputers. SoftwareX *1–2*, 19–25. https://doi.org/10.1016/j.softx.2015.06.001.

51. Hart, K., Foloppe, N., Baker, C.M., Denning, E.J., Nilsson, L., and Mackerell, A.D., Jr. (2012). Optimization of the CHARMM additive force field for DNA: Improved treatment of the BI/BII conformational equilibrium. J. Chem. Theor. Comput. *8*, 348–362. https://doi.org/10.1021/ct200723y.

52. Huang, J., Rauscher, S., Nawrocki, G., Ran, T., Feig, M., de Groot, B.L., Grubmüller, H., and MacKerell, A.D. (2017). CHARMM36m: an improved force field for folded and intrinsically disordered proteins. Nat. Methods *14*, 71–73. https://doi.org/10.1038/nmeth.4067.

53. Jorgensen, W.L., Chandrasekhar, J., Madura, J.D., Impey, R.W., and Klein, M.L. (1983). Comparison of simple potential functions for simulating liquid water. J. Chem. Phys. *79*, 926–935. https://doi.org/10.1063/1.445869.

54. Nawrocki, G., and Cieplak, M. (2013). Amino acids and proteins at ZnO-water interfaces in molecular dynamics simulations. Phys. Chem. Chem. Phys. *15*, 13628–13636. https://doi.org/10.1039/c3cp52198b.

55. Bussi, G., Donadio, D., and Parrinello, M. (2007). Canonical sampling through velocity rescaling. J. Chem. Phys. *126*, 014101. https://doi.org/10.1063/1.2408420.

56. Essmann, U., Perera, L., Berkowitz, M.L., Darden, T., Lee, H., and Pedersen, L.G. (1995). A smooth particle mesh Ewald method. J. Chem. Phys. *103*, 8577–8593. https://doi.org/10.1063/1.470117.

57. Miyamoto, S., and Kollman, P.A. (1992). Settle: an analytical version of the SHAKE and RATTLE algorithm for rigid water models. J. Comput. Chem. *13*, 952–962. https://doi.org/10.1002/jcc.540130805.

58. Hess, B., Bekker, H., Berendsen, H.J.C., and Fraaije, J.G.E.M. (1997). LINCS: a linear constraint solver for molecular simulations. J. Comput. Chem. *18*, 1463–1472. https://doi.org/10.1002/(sici)1096-987x(199709)18:12<1463::Aid-jcc4>3.0.Co;2-h.

59. Li, Z., Wang, Y., Xiang, S., Zheng, Z., Bian, Y., Feng, B., and Weng, X. (2020). Chondrocytes-derived exosomal miR-8485 regulated the Wnt/beta-catenin pathways to promote chondrogenic differentiation of BMSCs. Biochem. Biophys. Res. Commun. *523*, 506–513. https://doi.org/10.1016/j.bbrc.2019.12.065.

60. Liu, S., Chu, L., Xie, M., Ma, L., An, H., Zhang, W., and Deng, J. (2021). miR-92a-3p promoted EMT via targeting LATS1 in cervical cancer stem cells. Front. Cell Dev. Biol. *9*, 757747. https://doi.org/10.3389/fcell.2021.757747.

61. Zhu, L., and Mei, M. (2021). Interference of long non-coding RNA HAGLROS inhibits the proliferation and promotes the apoptosis of ovarian cancer cells by targeting miR-26b-5p. Exp. Ther. Med. *22*, 879. https://doi.org/10.3892/etm.2021.10311.

62. Yu, M., and Liu, J. (2020). MicroRNA-30d-5p promotes ovarian granulosa cell apoptosis by targeting Smad2. Exp. Ther. Med. *19*, 53–60. https://doi.org/10.3892/etm.2019.8184.

63. Liu, B., Yan, L., Chi, Y., Sun, Y., and Yang, X. (2021). Long non-coding RNA AFAP1-AS1 facilitates ovarian cancer progression by regulating the miR-107/PDK4 axis. J. Ovarian Res. *14*, 60. https://doi.org/10.1186/s13048-021-00808-x.

64. Yang, N., Kaur, S., Volinia, S., Greshock, J., Lassus, H., Hasegawa, K., Liang, S., Leminen, A., Deng, S., Smith, L., et al. (2008). MicroRNA microarray identifies let-7i as a novel biomarker and therapeutic target in human epithelial ovarian cancer. Cancer Res. *68*, 10307–10314. https://doi.org/10.1158/0008-5472.CAN-08-1954.

65. Biamonte, F., Santamaria, G., Sacco, A., Perrone, F.M., Di Cello, A., Battaglia, A.M., Salatino, A., Di Vito, A., Aversa, I., Venturella, R., et al. (2019). MicroRNA let-7g acts as tumor suppressor and predictive biomarker for chemoresistance in human epithelial ovarian cancer. Sci. Rep. *9*, 5668. https://doi.org/10.1038/s41598-019-42221-x.

66. Yoshimura, A., Sawada, K., Nakamura, K., Kinose, Y., Nakatsuka, E., Kobayashi, M., Miyamoto, M., Ishida, K., Matsumoto, Y., Kodama, M., et al. (2018). Exosomal miR-99a-5p is elevated in sera of ovarian cancer patients and promotes cancer cell invasion by increasing fibronectin and vitronectin expression in neighboring peritoneal mesothelial cells. BMC Cancer *18*, 1065. https://doi.org/10.1186/s12885-018-4974-5.

67. Du, W., Feng, Z., and Sun, Q. (2018). LncRNA LINC00319 accelerates ovarian cancer progression through miR-423-5p/NACC1 pathway. Biochem. Biophys. Res. Commun. *507*, 198–202. https://doi.org/10.1016/j.bbrc.2018.11.006.

68. Todeschini, P., Salviato, E., Paracchini, L., Ferracin, M., Petrillo, M., Zanotti, L., Tognon, G., Gambino, A., Calura, E., Caratti, G., et al. (2017). Circulating miRNA landscape identifies miR-1246 as promising diagnostic biomarker in high-grade serous ovarian carcinoma: a validation across two independent cohorts. Cancer Lett. *388*, 320–327. https://doi.org/10.1016/j.canlet.2016.12.017.

69. Cao, J., Zhang, Y., Mu, J., Yang, D., Gu, X., and Zhang, J. (2021). Exosomal miR-21-5p contributes to ovarian cancer progression by regulating CDK6. Hum. Cell *34*, 1185–1196. https://doi.org/10.1007/s13577-021-00522-2.

70. Otahal, A., Kuten-Pella, O., Kramer, K., Neubauer, M., Lacza, Z., Nehrer, S., and De Luna, A. (2021). Functional repertoire of EV-associated miRNA profiles after lipoprotein depletion via ultracentrifugation and size exclusion chromatography from autologous blood products. Sci. Rep. *11*, 5823. https://doi.org/10.1038/s41598-021-84234-5.

71. Gutiérrez García, G., Galicia García, G., Zalapa Soto, J., Izquierdo Medina, A., Rotzinger-Rodríguez, M., Casas Aguilar, G.A., López Pacheco, C.P., Aguayo, Á., and Aguilar-Hernandez, M.M. (2020). Analysis of RNA yield in extracellular vesicles isolated by membrane affinity column and differential ultracentrifugation. PLoS One *15*, e0238545. https://doi.org/10.1371/journal.pone.0238545.

72. Andreu, Z., Rivas, E., Sanguino-Pascual, A., Lamana, A., Marazuela, M., González-Alvaro, I., Sánchez-Madrid, F., de la Fuente, H., and Yáñez-Mó, M. (2016). Comparative analysis of EV isolation procedures for miRNAs detection in serum samples. J. Extracell. Vesicles *5*, 31655. https://doi.org/10.3402/jev.v5.31655.

73. Gaspar, L.S., Santana, M.M., Henriques, C., Pinto, M.M., Ribeiro-Rodrigues, T.M., Girão, H., Nobre, R.J., and Pereira de Almeida, L. (2020). Simple and fast SEC-based protocol to isolate human plasma-derived extracellular vesicles for transcriptional research. Mol. Ther. Methods Clin. Dev. *18*, 723–737. https://doi.org/10.1016/j.omtm.2020.07.012.

74. Kanwar, S.S., Dunlay, C.J., Simeone, D.M., and Nagrath, S. (2014). Microfluidic device (ExoChip) for on-chip isolation, quantification and characterization of circulating exosomes. Lab Chip *14*, 1891–1900. https://doi.org/10.1039/c4lc00136b.

75. Ozawa, P.M.M., Vieira, E., Lemos, D.S., Souza, I.L.M., Zanata, S.M., Pankievicz, V.C., Tuleski, T.R., Souza, E.M., Wowk, P.F., Urban, C.d.A., et al. (2020). Identification of miRNAs enriched in extracellular vesicles derived from serum samples of breast cancer patients. Biomolecules *10*, 150. https://doi.org/10.3390/biom10010150.